Cytokine 61 (2013) 578–584

Contents lists available at SciVerse ScienceDirect

Cytokine

journal homepage: www.journals.elsevier.com/cytokine

Mutants of lymphotoxin-α with augmented cytotoxic activity *via* TNFR1 for use in cancer therapy

Tomohiro Morishige [a,1], Yasuo Yoshioka [b,c,*,1], Shogo Narimatsu [a], Shinji Ikemizu [d], Shin-ichi Tsunoda [c,e], Yasuo Tsutsumi [b,c,e], Yohei Mukai [a], Naoki Okada [a], Shinsaku Nakagawa [a,c,*]

[a] *Laboratory of Biotechnology and Therapeutics, Graduate School of Pharmaceutical Sciences, Osaka University, 1-6 Yamadaoka, Suita, Osaka 565-0871, Japan*
[b] *Laboratory of Toxicology and Safety Science, Graduate School of Pharmaceutical Sciences, Osaka University, 1-6 Yamadaoka, Suita, Osaka 565-0871, Japan*
[c] *The Center for Advanced Medical Engineering and Informatics, Osaka University, 1-6 Yamadaoka, Suita, Osaka 565-0871, Japan*
[d] *Graduate School of Pharmaceutical Sciences, Kumamoto University, 5-1 Oe-honmachi, Kumamoto 862-0973, Japan*
[e] *Laboratory of Biopharmaceutical Research, National Institute of Biomedical Innovation, 7-6-8 Saito-Asagi, Ibaraki, Osaka 567-0085, Japan*

ARTICLE INFO

Article history:
Received 6 July 2012
Received in revised form 29 September 2012
Accepted 6 November 2012
Available online 11 December 2012

Keywords:
Affinity
Apoptosis
Bioactivity
Cytokine
Cytotoxicity

ABSTRACT

The cytokine lymphotoxin-α (LTα) is a promising candidate for use in cancer therapy. However, the instability of LTα *in vivo* and the insufficient levels of tumor necrosis factor receptor 1 (TNFR1)-mediated bioactivity of LTα limit its therapeutic potential. Here, we created LTα mutants with increased TNFR1-mediated bioactivity by using a phage display technique. We constructed a phage library displaying lysine-deficient structural variants of LTα with randomized amino acid residues. After affinity panning, we screened three clones of lysine-deficient LTα mutant, and identified a LTα mutant with TNFR1-mediated bioactivity that was 32 times that of the wild-type LTα (wtLTα). When compared with wtLTα, the selected clone showed augmented affinity to TNFR1 due to slow dissociation rather than rapid association. In contrast, the mutant showed only 4 times the TNFR2-mediated activity of wtLTα. In addition, the LTα mutant strongly and rapidly activated caspases that induce TNFR1-mediated cell death, whereas the mutant and wtLTα activated nuclear factor-kappa B to a similar extent. Our data suggest that the kinetics of LTα binding to TNFR1 play an important role in signal transduction patterns, and a TNFR1-selective LTα mutant with augmented bioactivity would be a superior candidate for cancer therapy.

1. Introduction

Lymphotoxin-alpha (LTα) is a tumor necrosis factor (TNF) superfamily cytokine with tumor-cell-specific cytotoxic activity and immune-activating activity. LTα induces the expression of chemokines and adhesion molecules in endothelial cells, and plays a key role in lymph node neogenesis [1–3]. Schrama et al. [4,5] showed that systemic administration of LTα to a tumor-bearing mouse leads to the construction of ectopic lymphoid tissue within the tumor and the strong induction of tumor immunity in that lymphoid tissue, suggesting that the underlying mechanism of this cytokine's anti-tumor activity may be effective. Therefore, LTα has long been considered to be a promising candidate for an anti-cancer agent. However, the clinical use of LTα has been limited because of the protein's *in vivo* instability and proinflammatory side effects.

One of the most common ways to improve the therapeutic effects of proteins is to conjugate them with polyethylene glycol (PEG) in a process called PEGylation, or to conjugate them with other water-soluble polymers [6]. Because of the steric hindrance caused by the PEG molecule, PEGylation can prolong the plasma half-life of molecules and alter the tissue distribution of the conjugates compared with those of the native form. PEGylation of proteins is mostly nonspecific because it targets all of the lysine residues in the protein, some of which may be in or near an active site. As a result, PEGylation significantly reduces the specific

Abbreviations: E. coli, Escherichia coli; ELISA, enzyme-linked immunosorbent assay; FADD, Fas-associated protein with death domain; FBS, fetal bovine serum; HVEM, herpes virus entry mediator; IFNγ, interferon γ; LTα, lymphotoxin-alpha; NFκB, nuclear factor-kappa B; PEG, polyethylene glycol; pI, isoelectric points; SDS-PAGE, sodium dodecyl sulfate–polyacrylamidegel electrophoresis; SPR, surface plasmon resonance; TNF, tumor necrosis factor; TNFR1, TNF receptor 1; TRADD, TNF receptor-associated death domain; TRAF, TNF receptor-associated factor; wtLTα, wild-type LTα.

* Corresponding authors. Addresses: Laboratory of Toxicology and Safety Science, Graduate School of Pharmaceutical Sciences, Osaka University, 1-6 Yamadaoka, Suita, Osaka 565-0871, Japan. Tel./fax: +81 6 6879 8233 (Y. Yoshioka), Laboratory of Biotechnology and Therapeutics, Graduate School of Pharmaceutical Sciences, Osaka University, 1-6 Yamadaoka, Suita, Osaka 565-0871, Japan. Tel.: +81 6 6879 8175; fax: +81 6 6879 8179 (S. Nakagawa).

E-mail addresses: yasuo@phs.osaka-u.ac.jp (Y. Yoshiokab), nakagawa@phs.osaka-u.ac.jp (S. Nakagawa).

[1] These authors contributed equally to the work.

1043-4666/$ - see front matter © 2012 Elsevier Ltd. All rights reserved.
http://dx.doi.org/10.1016/j.cyto.2012.11.005

activity of the proteins involved. Our group previously developed a novel strategy for site-specific mono-PEGylation of lysine-deficient mutants to overcome these limitations of PEGylation [7,8]. We demonstrated that site-specific PEGylation of a lysine-deficient mutant of LTα retained higher bioactivity compared with random PEGylation of wild-type LTα (wtLTα) [9]. This finding suggests that site-specific PEGylation of a lysine-deficient mutant of LTα might be a useful way to overcome the problems in the clinical use of LTα outlined above.

LTα binds to three receptor subtypes—TNF receptor 1 (TNFR1), TNFR2, and herpes virus entry mediator (HVEM)—to exert various biological functions. TNFR1 induces an anti-tumor effect and Peyer's patch development, whereas TNFR2 is essential for immune responses against bacteria and viruses [1]. Human LTα and TNF that bind to murine TNFR1, but not to murine TNFR2, are not lethal in healthy mice except at extremely high doses, suggesting that LTα and TNF α exhibit their lethal side effects *via* TNFR2 [10,11]. Therefore, LTα as a cancer immunotherapeutic agent, a LTα mutant with selectively increased TNFR1-mediated bioactivity is needed. Previously, we successfully created a TNFR1-selective LTα mutant whose bioactivity *via* TNFR1 was several times that of wtLTα, and whose bioactivity *via* TNFR2 was 2.5% that of wtLTα [12]. However, to enhance therapeutic efficacy and suppress the side effect of LTα, it is necessary to create a LTα mutant with greatly increased TNFR1-mediated bioactivity and TNFR1-selectivity.

In this study, we attempted to create LTα mutants with selectively increased TNFR1-mediated bioactivity by using a phage display technique. We succeeded in creating a LTα mutant that had a much higher bioactivity *via* TNFR1 and an augmented affinity to TNFR1 compared with that of wtLTα, and demonstrated that this was due to the slow dissociation rate of the LTα mutant-TNFR1 complex. In addition, we showed that the LTα mutant differed from wtLTα by its ability to strongly and rapidly activate caspases. In contrast, the LTα mutant and wtLTα were similar to each other in their degree of activation of nuclear factor-kappa B (NFκB). Our findings suggest that this LTα mutant would be a superior candidate for a cancer immunotherapeutic agent.

2. Materials and methods

2.1. Cells

HEp-2 cells, a human carcinoma cell line derived via HeLa contamination, were purchased from the American Type Culture Collection (Manassas, VA), and cultured in RPMI 1640 medium (Wako Pure Chemical Industries, Osaka, Japan) supplemented with 10% fetal bovine serum (FBS), 1 mM sodium pyruvate, 50 μM 2-mercaptoethanol, and antibiotics. HT29.14S cells, a TNF/LT-sensitive subclone of HT29 human colon adenocarcinoma, were kindly provided by Dr. Carl Ware (La Jolla Institute for Allergy and Immunology, CA) [13]. HT29.14S cells were cultured in Dulbecco's Modified Eagle's Medium (Wako Pure Chemical Industries) supplemented with 10% FBS, 10 mM HEPES, and antibiotics. hTNFR2/mFas-PA cells are preadipocytes derived from TNFR1$^{-/-}$ TNFR2$^{-/-}$ mice expressing a chimeric receptor composed of the extracellular and transmembrane domain of human TNFR2 and the intracellular domain of mouse Fas, which is a member of the TNF receptor superfamily [14]; these cells were cultured in RPMI 1640 medium supplemented with 10% FBS, 5 μg/mL Blasticidin S HCl (Invitrogen, Carlsbad, CA), and antibiotics. MCF-7 cells were provided from the Institute of Development, Aging and Cancer, Tohoku University, and were cultured in Eagle's Minimum Essential Medium (Wako Pure Chemical Industries) supplemented with 10% FBS, 0.01 mg/mL bovine insulin, and antibiotics.

2.2. Construction of a library of lysine-deficient mutants of LTα

The phagemid vector pY03′, which encodes human wtLTα with the C-terminus of wtLTα fused to the N-terminus of the M13 phage g3p, was used as a PCR template for constructing a DNA library of lysine-deficient mutants of LTα. We performed a two-step PCR amplification using oligonucleotides containing the sequence NNS (where N represents A, C, G, or T; and S represents C or G) at Lys19, Lys28, Lys39, Lys84, Lys89, and Lys119 of wtLTα; the sequence NNS encodes all 20 standard amino acids. The products from the second PCR were digested with *Nco*I and *Pst*I and then ligated into pY03′. The phagemid was electroporated into *Escherichia coli* (*E. coli*) TG1 cells (Stratagene, Cedar Creek, TX), yielding 2×10^6 independent clones. The phage library displaying lysine-deficient LTα molecules was prepared as described previously [12]. Briefly, pY03′-transformed TG1 cells were infected with M13KO7 helper phage (Invitrogen) and cultured for 6 h at 25 °C. The resultant phage particles were precipitated from the culture supernatant by using PEG (MP Biomedicals, Solon, OH) and suspended in NTE (100 mM NaCl, 10 mM Tris, 1 mM EDTA).

2.3. Selection of bioactive LTα mutants

Screening for bioactive LTα mutants was performed as described previously [12]. Briefly, an immunoplate was coated with soluble human TNFR1 (R&D Systems, Minneapolis, MN), and the prepared phage library was allowed to bind to the immobilized TNFR1. After a second round of panning, single colonies were picked and cultured. The resulting phage-containing culture supernatant was used for screening by enzyme-linked immunosorbent assay (ELISA) against human TNFR1.

2.4. Expression and purification of recombinant LTαs

pET15b plasmids (Novagen, Darmstadt, Germany) encoding LTαs were prepared and used to transform *E. coli* BL21(DE3) cells (Stratagene) for the expression of recombinant protein, as described previously [12]. Expression was induced by adding 1 mM isopropyl β-D-1-thiogalactopyranoside and incubating the cells at 37 °C for 6 h in Terrific Broth (Invitrogen Corporation, Carlsbad, CA) containing 0.4% glucose, 1.68 mM $MgSO_4$, and 100 μg/mL of ampicillin; all products were accumulated as inclusion bodies. The resultant inclusion bodies were washed, solubilized, reduced, and refolded by the methods previously described [12]. After dialysis against a buffer containing 20 mM Tris–HCl (pH 7.4) and 100 mM urea, active trimeric LTα proteins were purified by using a HiLoad Superdex 200PG column (GE Healthcare, UK) equilibrated with phosphate-buffered saline (pH 7.4) followed by ion-exchange chromatography (SP Sepharose Fast Flow for wtLTα; Q Sepharose Fast Flow for mutants of LTα); both columns were obtained from GE Healthcare. To create point mutants, we used pET15b-human wtLTα as a template with a KOD-plus mutagenesis kit (Toyobo, Osaka, Japan) according to the manufacturer's instructions. Recombinant point mutants were produced and purified as described earlier; SP Sepharose Fast Flow was used as the ion-exchange column. Protein concentration was measured by using Coomassie Protein Assay Reagent (Thermo Fisher Scientific, Rockford, IL). Sodium dodecyl sulfate–polyacrylamidegel electrophoresis (SDS–PAGE) analysis of LTαs was conducted under reducing conditions, and the proteins in the gels were stained with Coomassie brilliant blue. The electrostatic potential surface was generated by using GRASP software [15]. The electrostatic potential ranged from −7.5 kT to 7.5 kT. The relative accessible surface areas were calculated by using JOY software [16].

2.5. Cytotoxicity assays

HEp-2 cells were seeded at 4×10^4 cells per well in 96-well plates and incubated for 18 h with serially-diluted LTαs in the presence of 50 μg/mL cycloheximide. For the functional blocking assay, HEp-2 cells were treated with serially-diluted MAB225 (R&D Systems), an anti-TNFR1 antibody, for 30 min. The cells were then incubated with 100 ng/mL wtLTα and LTα mutants for 18 h in the presence of 50 μg/mL cycloheximide. For the caspase inhibition assay, HEp-2 cells were incubated with serially-diluted wtLTα or LTα mutants in the presence of 50 μg/mL cycloheximide and 50 mM zVAD-fmk (Calbiochem, Darmstadt, Germany) for 18 h. R2/Fas preadipocyte cells were seeded at 1.5×10^4 cells per well in 96-well plates and incubated for 48 h with serially-diluted LTαs in the presence of 50 μg/mL cycloheximide. The cytotoxicities of LTαs against HEp-2 cells and R2/Fas preadipocyte cells were assessed by using the standard methylene blue assay method as previously described [12]. HT29.14S and MCF-7 cells were seeded at 5×10^3 cells per well and incubated with LTαs in the presence of 80 U/mL human Interferon γ (IFNγ) (R&D Systems) for 72 h. After incubation, cell viability was measured by using a WST-8 assay kit (Nacalai Tesque, Kyoto, Japan) according to the manufacturer's instructions. The ratio of TNFR1-/TNFR2-mediated bioactivity was calculated as follows: activity of LTαs in HEp-2 cells/activity of LTαs in R2/Fas preadipocyte cells. The TNFR1/TNFR2 ratio for wtLTα was set equal to 1.

2.6. Analysis of binding kinetics by surface plasmon resonance

The binding kinetics of LTαs were analyzed and compared by using a surface plasmon resonance (SPR) method (BIAcore 2000, GE Healthcare, UK). Human TNFR1, TNFR2, or HVEM Fc chimera (R&D Systems, Inc.) was diluted to 50 μg/mL in 10 mM sodium acetate (pH 4.5) and immobilized onto a CM5 sensor chip by using an amine coupling kit (GE Healthcare, UK) as described previously [12]. During the association phase, wtLTα or LTα mutants diluted in HBS-EP running buffer (GE, Healthcare UK) to 37, 18.5, 9.3, 4.6, or 2.3 nM were passed over the immobilized TNFRs for 2 min at a flow rate 20 μL/min. During the dissociation phase, HBS-EP was run over the sensor chip for 1 min at a flow rate 20 μ L/min. Complexes were eluted by using 20 μL of 10 mM glycine–HCl (pH 2.0). Data were evaluated by using BIAevaluation 4.1 software (GE Healthcare UK) to apply a 1:1 Langmuir binding model. The obtained sensorgrams were fitted globally over the range of injected concentrations and simultaneously over the association and dissociation phases.

2.7. Evaluation of caspase-3/7 and -8 activities

HEp-2 cells were seeded at 4×10^4 cells per well in 96-well plates and then incubated for 6, 12, or 18 h with 10 ng/mL of the relevant LTα in the presence of 50 μg/mL cycloheximide. Activities of intracellular caspase-8 and caspase-3/7 were measured by using Caspase-Glo assays (Promega, Madison, WI) according to the manufacturer's instructions.

2.8. Evaluation of NFκB activities

HEp-2 cells were co-transfected with pGL4.32, a NFκB-responsive firefly luciferase expression vector, and pRL-TK, a thymidine kinase–regulated renilla luciferase expression vector (Promega) at a ratio of 90:1 for 18 h. The cells were then treated with 10 ng/mL of wtLTα or LTα mutants for 1, 2, 4, 6, 12, and 24 h. Expression levels of intracellular firefly luciferase and renilla luciferase were then measured by using the Dual-Luciferase Reporter Assay System (Promega). The expression level of firefly luciferase was normalized against that of renilla luciferase.

3. Results

3.1. Production of a highly bioactive LTα mutant

Our recent study showed that site-specific PEGylation of a lysine-deficient mutant of LTα might be useful for cancer therapy, because the mutant retained bioactivity after PEGylation [9]. Here, we attempted to create a lysine-deficient mutant of LTα with augmented bioactivity *via* TNFR1 and TNFR1-selective bioactivity that could be used for site-specific PEGylation in the future. A phage library displaying LTα mutants with randomized sequences in place of all lysine codons was prepared. For the construction of the phage library, two-step PCR was used to replace the lysine codons randomly with an NNS sequence. As a result, we successfully constructed a library with 2×10^6 independent clones, and performed two rounds of panning against immobilized human TNFR1; phage clones were screened for binding affinity to TNFR1 by conducting an ELISA (data not shown). We obtained three LTα mutants (mutLT1, mutLT2, and mutLT3), which were putative lysine-deficient mutants of LTα. DNA sequencing analysis of the LTα mutants confirmed that all 6 lysine residues present in wtLTα were mutated to other amino acids (Table 1). To investigate the properties of the LTα mutants in detail, we prepared recombinant LTα mutant proteins by using an *E. coli* expression system, as previously described [12]. LTα mutants and wtLTα were expressed in *E. coli* and obtained through refolding of inclusion bodies. Purified LTα mutants displayed a molecular mass of 18 kDa by SDS–PAGE analysis (Fig. 1A), and a molecular mass of approximately 60 kDa by size exclusion chromatography (Fig. 1B), indicating that LTα mutants form homotrimeric complexes, as does wtLTα. The isoelectric points (pI) of mutLT1, mutLT2, and mutLT3 were 6.16, 6.16, and 6.00, respectively whereas that of wtLTα was 8.94 (Table 1). We also visually assessed the changes in the surface electrostatic potential values by using GRASP software (Fig. 1C). Because of their lack of lysine residues, LTα mutants had more negative areas on their surface than did wtLTα.

3.2. Bioactivities of LTα mutants

To assess the TNFR1-mediated bioactivity of LTα mutants, cytotoxicity assays using HEp-2 cells were performed (Fig. 2A). wtLTα and LTα mutants showed dose-dependent cytotoxicity, and the bioactivity of each LTα mutant was higher than that of wtLTα in the HEp-2 cells (Fig. 2A). The bioactivity of mutLT1 was especially high (31.8 times that of wtLTα; Table 2). Furthermore, we confirmed that the LTα-induced cytotoxicity was blocked by the anti-TNFR1 antibody in all cases (Fig. 2B). These results indicate that the LTα mutants possess higher TNFR1-mediated bioactivity than that displayed by wtLTα. To confirm that the higher bioactivity of the LTα mutants was not specific to HEp-2 cells, we examined the bio-

Table 1
Amino acid sequences and the isoelectric points of LTα mutants. The pI values of LTαs were calculated by using a program in the Expert Protein Analysis System proteomics server of the Swiss Institute of Bioinformatics (Basel, Switzerland).

	Residue position						pI
	19	28	39	84	89	119	
wtLTα	Lys	Lys	Lys	Lys	Lys	Lys	8.94
mutLT1	Asn	Gln	Asn	Ser	Leu	Gly	6.16
mutLT2	Asn	Gln	Ser	Thr	Val	Val	6.16
mutLT3	Asp	Gln	Ala	Thr	Thr	Ala	6.00

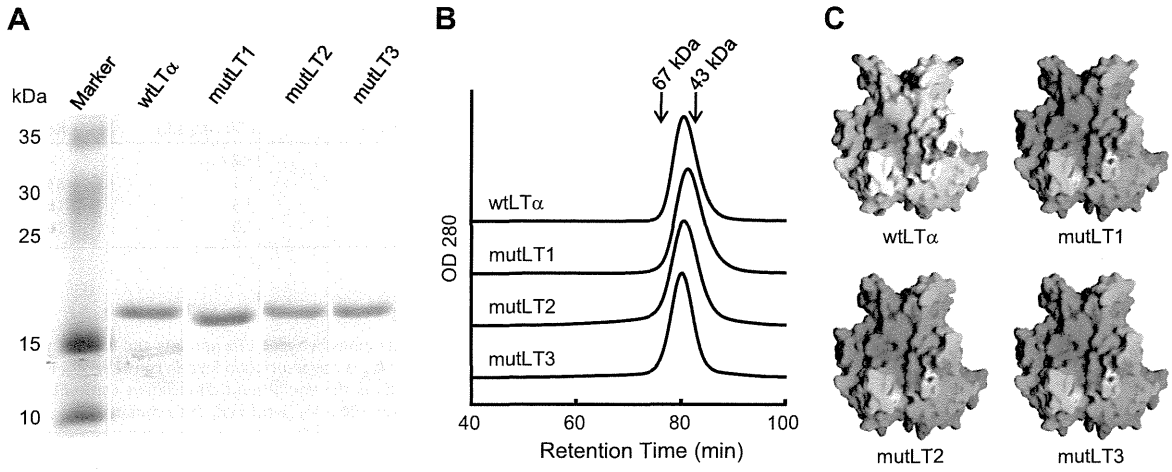

Fig. 1. Properties of recombinant LTα mutants. (A) SDS–PAGE analysis of wtLTα and LTα mutants. All products were separated on an SDS–PAGE gel and visualized by means of Coomassie Brilliant Blue staining. Marker indicates molecular weight standards. (B) Chromatograms of purified wtLTα and LTα mutants. wtLTα or LTα mutants were loaded onto a size-exclusion column and eluted at 1.0 mL/min. (C) The electrostatic potential surface was generated by using GRASP software. Red and blue indicate negative and positive electrostatic potentials, respectively. The electrostatic potential ranged from −7.5 kT (bright blue) to 7.5 kT (bright red). The relative accessible surface areas were calculated by using JOY software.

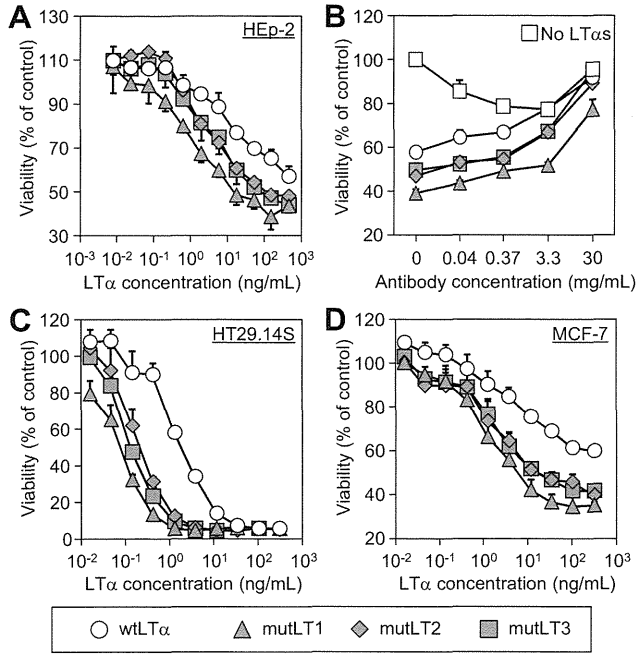

Fig. 2. TNFR1-mediated cytotoxic activity of wtLTα and LTα mutants. (A) HEp-2 cells were incubated with wtLTα or LTα mutants in the presence of cycloheximide. After 18 h incubation, cell viability was assessed by methylene blue assay. (B) HEp-2 cells were treated with serially-diluted MAB225, an anti-TNFR1 neutralizing antibody, for 30 min. The cells were then incubated with 100 ng/mL wtLTα or LTα mutants in the presence of cycloheximide. After 18 h incubation, the cell viability was assessed by methylene blue assay. (C) HT29.14S cells and (D) MCF-7 cells were incubated with wtLTα or LTα mutants in the presence of IFNγ. After 72 h incubation, the cell viability was assessed by WST-8 assay. EC30 and EC50 are the concentrations of LTα required for 30% and 50% inhibition of cell viability, respectively. Each value represents the mean ± SD ($n = 4$).

activities of mutLTαs in two other cell types (Fig. 2C and D, Table 2). When compared with wtLTα, the LTα mutants exhibited 8–24 times the cytotoxicity in HT29.14S cells, and 16–34 times the cytotoxicity in MCF-7 cells (Fig. 2C and D, Table 2). To specifically evaluate the TNFR2-mediated bioactivity of the LTα mutants, we examined the levels of cytotoxity induced by LTα mutants in hTNFR2/mFas-PA cells. These cells have been engineered to exhibit hTNFR2- but not hTNFR1-mediated activities [14]. The human TNFR2-mediated bioactivities of LTα mutants were 2.2–4.1 times those of wtLTα in hTNFR2/mFas-PA cells (Fig. 3). The calculated ratios of TNFR1-mediated bioactivity by using HEp-2 cells/TNFR2-mediated bioactivity induced by mutLT1, mutLT2, and mutLT3 were 7.8, 3.2, and 1.9 times that of wtLTα, respectively. This result suggests that LTα mutants, especially mutLT1, have selectivity for TNFR1 in addition to their augmented bioactivity.

Next, to measure the binding affinity of LTα mutants to TNFRs, we performed an SPR analysis by using a BIAcore 2000 biosensor (Table 3). The binding affinities of mutLT1, mutLT2 and mutLT3 to TNFR1 were 2.7, 2.0, and 1.4 times those of wtLTα, respectively. We considered that the increased affinity of LTα mutant for TNFR1 might be related to the enhanced bioactivity through this receptor. In particular, k_{off} values for LTα mutants binding to TNFR1 were 39–57% of the value for wtLTα, whereas the k_{on} values for LTα mutants binding to TNFR1 were almost the same as that for wtLTα. These results suggest that TNFR1 interacts more strongly with the LTα mutants than wtLTα due to slow dissociation kinetics, and that this binding mode between LTα mutant and TNFR1 induces a potent signaling pathway. We then evaluated the affinity of the LTα mutants for TNFR2 by using SPR methodology (Table 4). The affinity of TNFR2 for LTα mutants was 1.5–2.1 times that for wtLTα due to fast association kinetics. Taken together, these results indicate that the binding modes of LTα mutants to TNFR1 and TNFR2 might dictate their bioactivity.

We previously demonstrated that Lys84 in LTα plays a crucial role in the protein's interaction with the main chain of TNFR1 [12]. Therefore, to investigate the importance of the amino acid sequence at position 84, we created LTα mutants with Lys84 replaced by Ser84 (K84S), Thr84 (K84T), or Ala84 (K84A), and evaluated their binding kinetics and bioactivities *via* TNFR1. We found that these point mutants exhibited a slower dissociation rate and increased bioactivity *via* TNFR1 when compared with wtLTα. K84S showed especially high bioactivity even though its affinity for TNFR1 was lower than that of wtLTα (Table 5).

3.3. Activation of caspases by LTα mutant

It is known that TNFR1-mediated cell death is regulated by the activities of caspases including caspase-3, -7, and -8 [17].

Table 2
The TNFR1-mediated bioactivities of wtLTα and LTα mutants. EC30 and EC50 were calculated from the cytotoxic activity of wtLTα and LTα mutants against HEp-2, HT29.14S and MCF-7 cells. Relative activity values were calculated as EC30 (wtLTα)/EC30 (LTα mutant) or EC50 (wtLTα)/EC50 (LTα mutant).

	HEp-2 cells		HT29.14S cells		MCF-7 cells	
	EC30 (ng/mL)	Relative activity	EC50 (ng/mL)	Relative activity	EC50 (ng/mL)	Relative activity
wtLTα	47.7	1.0	1.80	1.0	36.7	1.0
mutLT1	1.5	31.8	0.08	23.6	1.1	33.7
mutLT2	6.8	7.0	0.21	8.5	2.3	16.0
mutLT3	7.8	6.1	0.13	14.2	2.3	16.0

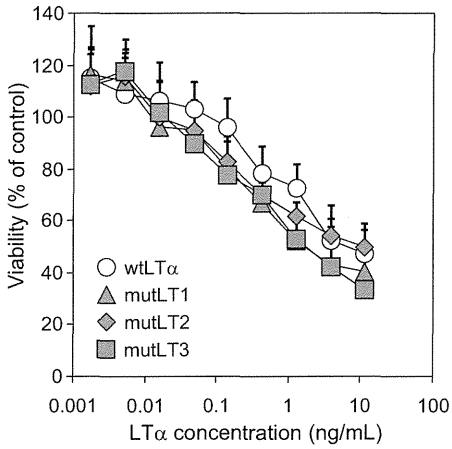

	EC30 (ng/mL)	Relative activity (% vs wtLTα)
wtLTα	1.39	100
mutLT1	0.34	409
mutLT2	0.64	217
mutLT3	0.43	323

Fig. 3. TNFR2-mediated cytotoxic activities of wtLTα and LTα mutants. hTNFR2/mFas-PA cells were incubated with serial dilutions of wtLTα or LTα mutants in the presence of cycloheximide. After 48 h incubation, cell viability was assessed by methylene blue assay. EC30 is the concentration of LTα required for 30% inhibition of cell viability. Each value represents the mean ± SD ($n = 4$).

Table 3
The binding kinetics of interactions between LTα mutants and hTNFR1 analyzed by using an SPR biosensor. k_{on} is the association kinetic constant; k_{off} is the dissociation kinetic constant; and K_D is the equilibrium dissociation constant. Relative affinity values were calculated as 100 × K_D (wtLTα)/K_D (LTα mutant).

	k_{on} (10^6/M s)	k_{off} (10^{-4}/s)	K_D (10^{-10}/M)	Relative affinity (% vs wtLTα)
wtLTα	1.2	6.1	4.9	100
mutLT1	1.3	2.4	1.8	269
mutLT2	1.4	3.5	2.5	195
mutLT3	0.97	3.4	3.4	143

Therefore, to examine the mechanism behind the augmentation of TNFR1-mediated bioactivity, we investigated the association between caspase activity and LTα mutant-induced cell death. First, we treated cells with LTα mutants in the presence of a broad caspase inhibitor, zVAD-fmk, and analyzed the cell viability (Fig. 4A). The results showed that zVAD-fmk almost completely abrogated the cytotoxicity induced by wtLTα and LTα mutants. These results indicate that both wild-type and LTα mutant-induced cell death were dependent on the activation of caspase. We then examined the activity of caspase-3/7 (Fig. 4B) and -8 (Fig. 4C) induced by LTα mutants in HEp-2 cells. LTα mutants, especially

Table 4
Binding kinetics of interactions between LTα mutants and hTNFR2 were analyzed by using an SPR biosensor. k_{on} is the association kinetic constant; k_{off} is the dissociation kinetic constant; and K_D is the equilibrium dissociation constant. Relative affinity values were calculated as 100 × K_D (wtLTα)/K_D (LTα mutant).

	k_{on} (10^6/M s)	k_{off} (10^{-4}/s)	K_D (10^{-10}/M)	Relative affinity (% vs wtLTα)
wtLTα	2.8	23.5	8.3	100
mutLT1	4.7	25.0	5.4	154
mutLT2	6.2	24.0	3.9	213
mutLT3	4.5	25.3	5.6	148

mutLT1, which has the highest bioactivity, quickly and strongly induced the activation of caspases. These results suggest that stabilization of the LTα -TNFR1 complex by the presence of LTα mutant contributed to increased caspase activity, which in turn induced cytotoxic effects.

3.4. Activation of NFκB by LTα mutants

It is well known that TNFR1 activates NFκB signaling pathway in addition to the caspase cascade [18,19]. Therefore, to investigate whether the LTα mutants activate NFκB, we assessed the association between NFκB activity and LTα mutant-induced cell death. First, we prepared cells transfected with luciferase expressing vector activated by NFκB. Then, we treated cells with LTα mutants and analyzed the NFκB activity by measuring the expression level of luciferase (Fig. 5). Despite the higher TNFR1-mediated bioactivity of LTα mutants, we found that NFκB activity was induced to a similar extent by LTα mutants and wtLTα. This finding indicates that the LTα mutants selectively activate the caspase cascade but not NFκB activation *via* TNFR1.

4. Discussion

When constructing a LTα mutant as an anti-cancer agent, it is important that the mutant exhibits TNFR1 selectivity because of the lethal side-effects of TNFR2-mediated bioactivity. We previously created a LTα mutant (R1selLT), which had only 2.5% of the TNFR2-mediated bioactivity of wtLTα and 3.5 times of the TNFR1-mediated bioactivity of wtLTα [12]. The ratio of TNFR1/TNFR2 bioactivity of R1selLT was 145.8 times that of wtLTα. In addition to TNFR1 selectivity, augmentation of TNFR1-mediated bioactivity is also highly desirable in a therapeutic agent for cancer. Here, we created three lysine-deficient LTα mutants with greatly increased levels of TNFR1-mediated bioactivity through an altered binding mode. These mutants showed preferentially augmented bioactivity *via* TNFR1 compared with TNFR2. The TNFR1 selectivity of mutLT1, 2, and 3 was 7.8, 3.2, and 1.9 times that of wtLTα, respectively. Although the TNFR1 selectivity was lower for mutLT1 than for R1selLT, the TNFR1-mediated bioactivity of mutLT1 was 31.8 times that of wtLTα compared to 3.5 times of R1selLT. Such extreme augmentation of bioactivity is rarely reported. As

Table 5
Binding kinetics of interactions between point-mutated LTαs and hTNFR1 were analyzed by using an SPR biosensor. k_{on} is the association kinetic constant; k_{off} is the dissociation kinetic constant; and K_D is the equilibrium dissociation constant. Relative affinity values were calculated as 100 × K_D (wtLTα)/K_D (point mutated LTα). TNFR1-mediated relative activities of LTα mutants were calculated from the concentration of LTα required for 30% inhibition of HEp-2 cell viability.

	k_{on} (10^6/M s)	k_{off} (10^{-4}/s)	K_D (10^{-10}/M)	Relative affinity (% vs wtLTα)	Relative activity(% vs wtLTα)
wtLTα	1.2	6.1	4.9	100	100
K84S	0.28	2.2	8.0	62	4810
K84T	1.0	4.3	118	195	1100
K84A	1.5	5.3	3.5	143	910

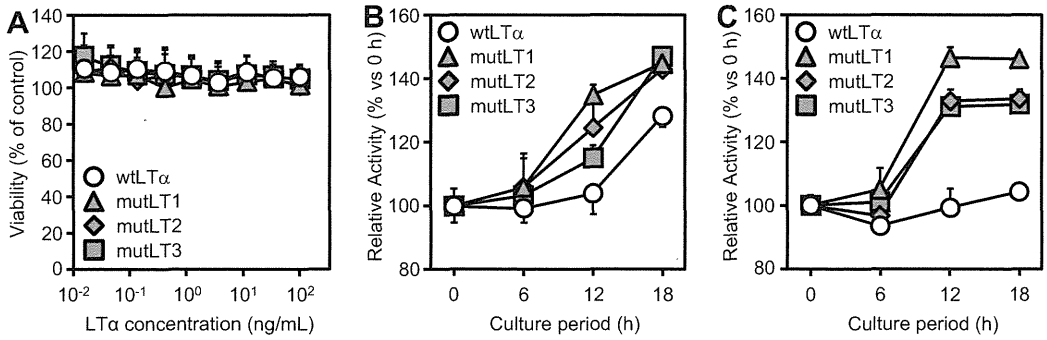

Fig. 4. Caspase activities in HEp-2 cells treated with wtLTα or LTα mutants. (A) Cycloheximide treated HEp-2 cells were incubated with wtLTα or LTα mutants in the presence of zVAD-fmk. After 18 h incubation, cell viability was assessed by methylene blue assay. (B and C) Cycloheximide treated HEp-2 cells were incubated for 6, 12, or 18 h with 10 ng/mL LTαs, and the activities of intracellular caspase-3/7 (B) and intracellular caspase-8 (C) were measured by using Caspase-Glo assays. Each value represents the mean ± SD (n = 4).

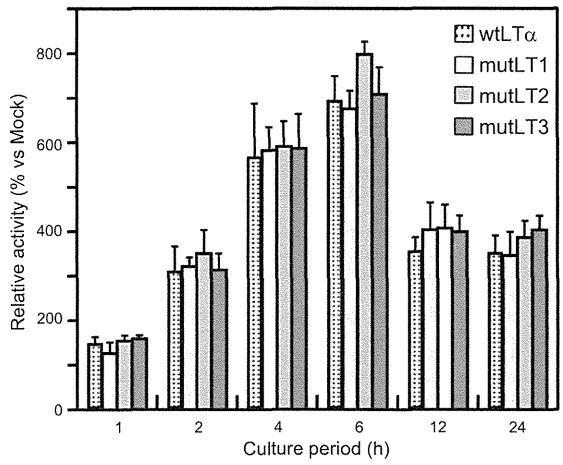

Fig. 5. NFκB activities in HEp-2 cells treated with wtLTα or LTα mutants. HEp-2 cells were co-transfected with pGL4.32 and pRL-TK (Promega). Eighteen hours after transfection, the cells were treated with 10 ng/mL LTαs for the indicated period. The intracellular luciferase activity was then quantified. Data are shown as the relative NFκB activity compared with the mock-transfected group. Each bar represents the mean ± SD (n = 4).

described above, high TNFR1 selectivity of R1selLT was mainly resulted from the significant decreased TNFR2-mediated bioactivity. On the other hand, the TNFR1 selectivity of mutLT1 was obtained from the augmented TNFR1-mediated bioactivity, while TNFR2-mediated bioactivity was maintained. On this point, TNFR2 is known to play essential role for the induction of immune responses. Therefore, we consider that a TNFR1-selective LTα mutants with high TNFR1-mediated and equivalent TNFR2-mediated bioactivity compared to wtLTα, such as mutLT1, would be a superior candidate for cancer therapy by combination of direct pro-apoptotic effects of LTα on tumor cells and an enhancement of local/systemic immunity.

Many cellular signaling processes are hypothesized to depend not only on the equilibrium strength of the ligand–receptor interactions but also on the average durations or kinetic dissociation rates of these interactions [20–23]. In some cases, the intensity of distal signaling depends on the off-rate rather than on the on-rate of the ligand–receptor complex [20,22]. For interactions with TNFR1, the LTα mutants exhibited higher k_{off} values compared with the value for wtLTα, whereas the k_{on} values for the LTα mutants were almost same as that for wtLTα. In addition, the bioactivity of wtLTα and LTα mutants was related to k_{off} but not to k_{on}. These data suggest that the LTα mutants interact with TNFR1 by slow dissociation and induce robust signal transduction. In contrast, for interactions with TNFR2, the LTα mutants showed a higher k_{on} than that for wtLTα, whereas the k_{off} values for the LTα mutants was almost same as that for wtLTα. These data indicate that the detailed molecular dissection of ligand-receptor binding kinetics is important for the construction of functional LTα mutants with desired TNFR-mediated bioactivity.

We previously demonstrated that Lys84 of LTα plays a crucial role in the protein's interaction with the main chain of TNFR1 [12]. Here, to explore the role of Lys84 further, we created LTα mutants with Lys84 replaced by Ser84 or Thr84, and found that the mutant with Ser84 showed slower dissociation kinetics and increased bioactivity when compared with wtLTα or the other mutants (Table 5). These results suggest that Lys84 contributes to the TNFR1-mediated bioactivity and the binding kinetics of the TNFR1–LTα interaction. In all three mutants analyzed here, the amino acid Lys at position 28 was changed to Gln (Table 1). Whereas these mutants exhibited increased TNFR1-mediated bioactivity, our previous data showed that a mutant with a K28Q substitution had decreased TNFR1-mediated bioactivity compared with that of wtLTα. Furthermore, mutLT2, which has the Lys at position 39 replaced by Ser, showed slightly increased TNFR2-mediated bioactivity, but a mutant containing the equivalent substitution at the same position showed decreased TNFR2-mediated bioactivity in our previous study [12]. These results suggest

that the sum of the mutations, including those at positions 28 and 39, were responsible for the augmented binding affinities to TNFR1 and TNFR2.

TNFR1 triggers apoptotic caspase signaling following activation of Fas-associated protein with death domain (FADD) [17]. At the same time, triggering of TNFR1 signals induces the anti-apoptotic NFκB cascade following the activation of TNF receptor-associated death domain (TRADD) and TNF receptor-associated factor (TRAF) adaptors [18,19,24]. Active NFκB induces transcription of a set of genes encoding anti-apoptotic proteins [25,26]. Therefore, in many cell types, TNF α has no apoptotic effects due to the parallel triggering by TNF α of a signaling pathway that activates NFκB *via* the TRADD and TRAF adaptors. Here, however, we found that the LTα mutants, which showed augmented bioactivity *via* TNFR1, efficiently induced caspase activation but induced NFκB to the same level as that induced by wtLTα (Figs. 4 and 5). We consider that the slower rate of dissociation of the LTα mutants from TNFR1 was important to the activation of FADD signaling cascade, but not to the activation of TRADD and TRAF adaptors. We speculate that the alteration of the binding mode of LTα mutant to TNFR1 increased the caspase signaling pathway, but not TRADD- and TRAF-mediated NFκB signaling. These findings will facilitate the construction of functional LTα mutants with even higher receptor selectivity and bioactivity in the future.

5. Conclusions

Here, we created highly bioactive LTα mutants with TNFR1-selectivity by using a phage display technique, and we clarified the molecular basis of their augmented TNFR1-mediated bioactivity. A better understanding of the correlation between structure, kinetic behavior, and activity will likely accelerate drug discovery because it will increase awareness of the properties of therapeutic proteins. We suggest that LTα mutants have the potential to be a powerful tool for cancer therapy by combination of direct pro-apoptotic effects of LTα on tumor cells and an enhancement of local/systemic immunity, and that our findings provide valuable information for the construction of even more functional LTα mutants.

Acknowledgements

The authors declare that they have no conflict of interests. This study was supported in part by grants from the Ministry of Health, Labor, and Welfare in Japan; by the Research on Health Sciences focusing on Drug Innovation from the Japan Health Sciences Foundation; and by the Takeda Science Foundation.

References

[1] Neumann B, Luz A, Pfeffer K, Holzmann B. Defective Peyer's patch organogenesis in mice lacking the 55-kD receptor for tumor necrosis factor. J Exp Med 1996;184:259–64.
[2] Kratz A, Campos-Neto A, Hanson MS, Ruddle NH. Chronic inflammation caused by lymphotoxin is lymphoid neogenesis. J Exp Med 1996;183:1461–72.
[3] Koni PA, Sacca R, Lawton P, Browning JL, Ruddle NH, Flavell RA. Distinct roles in lymphoid organogenesis for lymphotoxins alpha and beta revealed in lymphotoxin beta-deficient mice. Immunity 1997;6:491–500.
[4] Schrama D, thor Straten P, Fischer WH, McLellan AD, Brocker EB, Reisfeld RA, et al. Targeting of lymphotoxin-alpha to the tumor elicits an efficient immune response associated with induction of peripheral lymphoid-like tissue. Immunity 2001;14:111–21.
[5] Schrama D, Voigt H, Eggert AO, Xiang R, Zhou H, Schumacher TN, et al. Immunological tumor destruction in a murine melanoma model by targeted LTalpha independent of secondary lymphoid tissue. Cancer Immunol Immunother 2008;57:85–95.
[6] Ryan SM, Mantovani G, Wang X, Haddleton DM, Brayden DJ. Advances in PEGylation of important biotech molecules: delivery aspects. Expert Opin Drug Deliv 2008;5:371–83.
[7] Yamamoto Y, Tsutsumi Y, Yoshioka Y, Nishibata T, Kobayashi K, Okamoto T, et al. Site-specific PEGylation of a lysine-deficient TNF-alpha with full bioactivity. Nat Biotechnol 2003;21:546–52.
[8] Shibata H, Yoshioka Y, Ikemizu S, Kobayashi K, Yamamoto Y, Mukai Y, et al. Functionalization of tumor necrosis factor-alpha using phage display technique and PEGylation improves its antitumor therapeutic window. Clin Cancer Res 2004;10:8293–300.
[9] Narimatsu S, Yoshioka Y, Watanabe H, Masano T, Morishige T, Yao X, et al. Lysine-deficient lymphotoxin-alpha mutant for site-specific PEGylation. Cytokine 2011;56:489–93.
[10] Everaerdt B, Brouckaert P, Shaw A, Fiers W. Four different interleukin-1 species sensitize to the lethal action of tumour necrosis factor. Biochem Biophys Res Commun 1989;163:378–85.
[11] Brouckaert P, Libert C, Everaerdt B, Fiers W. Selective species specificity of tumor necrosis factor for toxicity in the mouse. Lymphokine Cytokine Res 1992;11:193–6.
[12] Yoshioka Y, Watanabe H, Morishige T, Yao X, Ikemizu S, Nagao C, et al. Creation of lysine-deficient mutant lymphotoxin-alpha with receptor selectivity by using a phage display system. Biomaterials 2010;31:1935–43.
[13] Browning JL, Miatkowski K, Sizing I, Griffiths D, Zafari M, Benjamin CD, et al. Signaling through the lymphotoxin beta receptor induces the death of some adenocarcinoma tumor lines. J Exp Med 1996;183:867–78.
[14] Abe Y, Yoshikawa T, Kamada H, Shibata H, Nomura T, Minowa K, et al. Simple and highly sensitive assay system for TNFR2-mediated soluble- and transmembrane-TNF activity. J Immunol Methods 2008;335:71–8.
[15] Nicholls A, Sharp KA, Honig B. Protein folding and association: insights from the interfacial and thermodynamic properties of hydrocarbons. Proteins 1991;11:281–96.
[16] Mizuguchi K, Deane CM, Blundell TL, Johnson MS, Overington JP. JOY: protein sequence-structure representation and analysis. Bioinformatics 1998;14:617–23.
[17] Sheikh MS, Huang Y. Death receptor activation complexes: it takes two to activate TNF receptor 1. Cell Cycle 2003;2:550–2.
[18] Chen G, Goeddel DV. TNF-R1 signaling: a beautiful pathway. Science 2002;296:1634–5.
[19] Magne N, Toillon RA, Bottero V, Didelot C, Houtte PV, Gerard JP, et al. NF-kappaB modulation and ionizing radiation: mechanisms and future directions for cancer treatment. Cancer Lett 2006;231:158–68.
[20] Hlavacek WS, Redondo A, Metzger H, Wofsy C, Goldstein B. Kinetic proofreading models for cell signaling predict ways to escape kinetic proofreading. Proc Nat Acad Sci USA 2001;98:7295–300.
[21] Liu ZJ, Haleem-Smith H, Chen H, Metzger H. Unexpected signals in a system subject to kinetic proofreading. Proc Nat Acad Sci USA 2001;98:7289–94.
[22] Krippner-Heidenreich A, Tubing F, Bryde S, Willi S, Zimmermann G, Scheurich P. Control of receptor-induced signaling complex formation by the kinetics of ligand/receptor interaction. J Biol Chem 2002;277:44155–63.
[23] Torigoe C, Faeder JR, Oliver JM, Goldstein B. Kinetic proofreading of ligand–FcepsilonRI interactions may persist beyond LAT phosphorylation. J Immunol 2007;178:3530–5.
[24] Kim JY, Lee JY, Kim DG, Koo GB, Yu JW, Kim YS. TRADD is critical for resistance to TRAIL-induced cell death through NF-kappaB activation. FEBS Lett 2011;585:2144–50.
[25] Arch RH, Gedrich RW, Thompson CB. Tumor necrosis factor receptor-associated factors (TRAFs) – a family of adapter proteins that regulates life and death. Genes Dev 1998;12:2821–30.
[26] Deveraux QL, Reed JC. IAP family proteins–suppressors of apoptosis. Genes Dev 1999;13:239–52.

Neuroscience Letters 534 (2013) 85–89

Contents lists available at SciVerse ScienceDirect

Neuroscience Letters

journal homepage: www.elsevier.com/locate/neulet

Proteomic analysis of the hippocampus in Alzheimer's disease model mice by using two-dimensional fluorescence difference in gel electrophoresis

Masaoki Takano[a], Takuya Yamashita[b,c], Kazuya Nagano[c], Mieko Otani[a], Kouji Maekura[a], Haruhiko Kamada[c], Shin-ichi Tsunoda[c], Yasuo Tsutsumi[b,c], Takami Tomiyama[e,f], Hiroshi Mori[e,f], Kenji Matsuura[d], Shogo Matsuyama[d,*]

[a] Laboratory of Molecular Cellular Biology, School of Pharmaceutical Sciences, Kobe Gakuin University, 1-1-3 Minatojima, Chuo-ku, Kobe 650-8586, Japan
[b] Laboratory of Toxicology and Safety Science, Graduate School of Pharmaceutical Sciences, Osaka University, 1-6 Yamadaoka, Suita, Osaka 565-0871, Japan
[c] Laboratory of Biopharmaceutical Research, National Institute of Biomedical Innovation, 7-6-8 Saito-Asagi, Ibaraki, Osaka 567-0085, Japan
[d] Faculty of Pharmaceutical Sciences, Himeji Dokkyo University, 7-2-1 Kamiohno, Himeji 670-8524, Japan
[e] Department of Neuroscience, Osaka City University Graduate School of Medicine, Osaka 545-8585, Japan
[f] Core Research for Evolutional Science and Technology, Japan Science and Technology Agency, Japan

HIGHLIGHTS

- We perform the proteome for $APP_{E693\Delta}$-transgenic mice. Methods are two-dimensional fluorescence difference in gel electrophoresis and mass spectrometry techniques. The expression of 14 proteins are changed in the brain. Aβ oligomers contribute to the expression of proteins.

ARTICLE INFO

Article history:
Received 4 August 2012
Received in revised form 13 October 2012
Accepted 6 November 2012

Keywords:
Proteome
Amyloid β oligomers
Alzheimer's disease
Hippocampus
2D-DIGE

ABSTRACT

We previously identified the E693Δ mutation in amyloid precursor protein (APP) in patients with Alzheimer's disease (AD) and then generated APP-transgenic mice expressing this mutation. As these mice possessed abundant Aβ oligomers from 8 months of age but no amyloid plaques even at 24 months of age, they are a good model to study pathological effects of amyloid β (Aβ) oligomers. The two-dimensional fluorescence difference in gel electrophoresis (2D-DIGE) technology, using a mixed-sample internal standard, is now recognized as an accurate method to determine and quantify proteins. In this study, we examined the proteins for which levels were altered in the hippocampus of 12-month-old $APP_{E693\Delta}$-transgenic mice using 2D-DIGE and liquid chromatography–tandem mass spectrometry (LC–MS/MS). Fourteen proteins were significantly changed in the hippocampus of $APP_{E693\Delta}$-transgenic mice. Actin cytoplasmic 1 (β-actin), heat shock cognate 71 kDa, γ-enolase, ATP synthase subunit β, tubulin β-2A chain, clathrin light chain B (clathrin) and dynamin-1 were increased. Heat shock-related 70 kDa protein 2, neurofilament light polypeptide (NFL), stress-induced-phosphoprotein 2, 60 kDa heat shock protein (HSP60), α-internexin, protein kinase C and casein kinase substrate in neurons protein 1 (Pacsin 1), α-enolase and β-actin were decreased. Western blotting also validated the changed levels of HSP60, NFL, clathrin and Pacsin 1 in $APP_{E693\Delta}$-transgenic mice. The identified proteins could be classified as cytoskeleton, chaperons, neurotransmission, energy supply and signal transduction. Thus, proteomics by 2D-DIGE and LC–MS/MS has provided knowledge of the levels of proteins in the early stages of AD brain.

1. Introduction

AD is neuropathologically characterized by abnormal accumulation of extracellular amyloid plaques and intracellular neurofibrillary tangles throughout cortical and limbic regions. Although the current amyloid cascade hypothesis [6] and tau hypothesis [15] provide frameworks for studying AD pathogenesis. Recently, diverse lines of evidence suggest that Aβ peptides play more important roles in AD pathogenesis [13,16,20]. Especially, soluble oligomers of Aβ could be a cause of synaptic and cognitive dysfunction in the early stages of AD. To address the relationship between Aβ oligomers and pathological features of AD, we generated APP transgenic mice expressing the E693Δ mutation, which enhanced Aβ oligomerization without fibrillization [25]. It might provide a clue for elucidating AD pathology caused by Aβ oligomers to analyze the $APP_{E693\Delta}$-transgenic mice.

* Corresponding author. Tel.: +81 79 223 6849; fax: +81 79 223 6857.
E-mail address: shogo@himeji-du.ac.jp (S. Matsuyama).

0304-3940/$ – see front matter © 2012 Elsevier Ireland Ltd. All rights reserved.
http://dx.doi.org/10.1016/j.neulet.2012.11.010

One of the most utilized approaches in proteomics to quantify and identify proteins is two dimensional gel electrophoresis (2DE) and mass spectrometry (MS) [5]. Proteomic approaches were most widely based on methods using differential expression on 2D-PAGE gels, or more recently 2D chromatography, followed by mass spectrometry protein identification. Compared to these conventional analyses, 2D-DIGE has higher reproducibility and sensitivity because of its internal standard design which minimizes gel-to-gel variation, improves spot matching, reduces number of gels needed, and permits quantitative analysis of small sample amounts.

In this study, we studied the altered expression of proteins in the hippocampus of $APP_{E693\Delta}$-transgenic mice using 2D-DIGE and LC–MS/MS approach. This approach revealed that the levels of at least 14 proteins were altered in the hippocampus of 12-month-old $APP_{E693\Delta}$-transgenic mice. These findings suggest that Aβ oligomers might cause synaptic and cognitive dysfunction by affecting the expression of these proteins in the hippocampus.

2. Experimental procedures

2.1. Materials

Sodium dodecyl sulfate, urea, thiourea, CHAPS, dithiothreitol, iodoacetamide, bromophenol blue, and RNase A and DNase I for SDS-PAGE or 2DE were all obtained from Wako Pure Chemical Industries (Osaka, Japan). Source information for all other assay reagents and materials are incorporated into their respective assay methods described below.

2.2. Animal subjects

Transgenic mice expressing human APP_{695} with the APP E693Δ mutation under the mouse prion promoter were used [25]. Heterozygous human $APP_{E693\Delta}$-transgenic mice and age-matched non-transgenic littermates were sacrificed at 12 months of age, and their hippocampi were isolated on an ice-cold plate. Animal care and handling were performed strictly in accordance with the Guidelines for Animal Experimentation at Kobe Gakuin University and Himeji Dokkyo University. Every effort was made to minimize the number of animals used and their suffering.

2.3. Protein labeling with CyDyes

Equal amounts of total protein from 4 hippocampi of $APP_{E693\Delta}$-transgenic mice or age-matched non-transgenic littermates were separately pooled. Protein samples were labeled with CyDyes (GE Healthcare, Piscataway, NJ), as per manufacturer's instructions. In brief, 50 μg of total protein from each sample was mixed in a tube and labeled with Cy2 minimal dye, and 50 μg protein taken from the mix was used as an internal standard on each gel for the three subsequent 2DE and image analysis. In parallel, 50 μg protein from each sample was labeled with either Cy3 or Cy5, and the dyes scrambled within each group to avoid possible dye bias. As a result, one replicate was Cy3 labeled proteins and another replicate was Cy5 labeled proteins. Two replicates (Cy3 and Cy5 labeled samples) were mixed, divided and applied each three independent gels. The sample volumes were adjusted to 18 μL with labeling buffer (7M urea, 2 M thiourea, 4% CHAPS, 30 mM Tris), followed by addition of 1 μL dye (working solution) to each individual sample. The samples were left on ice for 30 min in the dark, followed by adding 1 μL of 10 mmol/L lysine to stop the reaction.

2.4. 2D electrophoresis and image analysis

One sample from each of the CyDye groups was mixed together and adjusted to final concentrations of 1% DTT, 1% IPG buffer at a total volume of 350 μL with lysis buffer (7 M urea, 2 M thiourea, 4% CHAPS) and was used to 24 cm pH 4–7 IPG strips (non-linear; GE Healthcare, Piscataway, NJ) overnight. First dimension isoelectric focusing (IEF) was carried out with IPGphor II (GE Healthcare, Piscataway, NJ). Second dimension SDS-PAGE was performed by mounting the IPG strips onto 20 × 26 cm 12.5% DIGE gels (GE Healthcare, Piscataway, NJ) using Ettan DALT six Large Electrophoresis System (GE Healthcare, Piscataway, NJ) and running the gels at 16 mA/gel for the initial hour and 25 mA/gel at 25 °C constantly until bromophenol blue reached the bottom of the gel. The lysates were labeled at the ratio of 50 μg proteins: 400 pmol Cy3 or Cy5 protein-labeling dye (GE HealthcareBiosciences) in dimethylformamide according to the manufacturer's protocol.

In summary, three analytical gels were completed in total, running 25 μg of pooled reference sample labeled with Cy2, along with two samples (25 μg each), one labeled with Cy3 and the other labeled with Cy5. Gels selected for picking were stained with Deep purple (GE Healthcare, Piscataway, NJ). Approximately 1100 spots were matched across all three analytical gels. The analytical gel was picked using an automated robotic system, Ettan Spot picker (GE Healthcare, Piscataway, NJ). The pick list was created based on the Deep purple image. 2 mm gel plugs were picked, washed, reduced and alkylated, and then digested with trypsin, and the resulting peptides were extracted. Gel trypsinization was performed as previously described [24].

2.5. LC/MS/MS identification

Trypsinized peptides were analyzed by nano LC/MS/MS on a ThermoFisher LTQ Orbitrap XL. In brief, 30 mL of hydrolysate was loaded onto a 5 mm 675 mm ID C12 (Jupiter Proteo, Phenomenex) vented column at a flow-rate of 10 mL/min. Gradient elution was conducted on a 15 cm by 75 mm ID C12 column at 300 nL/min. A 30 min gradient was employed. The mass spectrometer was operated in a data-dependent mode, and the six most abundant ions were selected for MS/MS. Mass spectrometry results were searched using Mascot (www.matrixscience.com). Samples were processed in the Scaffold algorithm using DAT files generated by Mascot. Parameters for LTQ Orbitrap XL data require a minimum of two peptide matches per protein with minimum probabilities of 90% at the protein level.

2.6. Western blotting

Approximately 25 μg of protein from mouse hippocampus was applied to a 12.5% acrylamide gel and SDS-polyacrylamide gel electrophoresis was performed at 17.5 mA/gel for 2 h in second dimension. The gels were transferred onto PVDF membranes (Pall Corporation, Pensacola, FL, USA), in a trans-blot electrophoresis transfer cell (Nihon Eido, Tokyo, Japan). Western blotting was performed by using monoclonal antibodies against β-actin (diluted 1:1000, Cell Signaling, USA) and clathrin (diluted 1:250, Abcam, USA), polyclonal antibodies HSP60, NFL, voltage-dependent anion-selective channel protein 1 (VDAC) (diluted 1:1000, Cell Signaling, USA) and Pacsin 1 (diluted 1:500, Millipore, USA). Peroxidase-conjugated antibody (diluted 1:5000, Abcam, USA) was used as secondary antibody. The reaction was detected by chemiluminescence with ECL reagents (Pierce Biotechnology, USA). A semi quantitative analysis based on optical density was performed by ImageJ software (available at http://www.rsbweb.nih.gov/ij).

3. Results and discussion

The 2D-DIGE gels of the hippocampi from wild type and $APP_{E693\Delta}$-transgenic mice pools were shown as Fig. 1. Two replicates of each pooled sample were run, labeling one replicate with

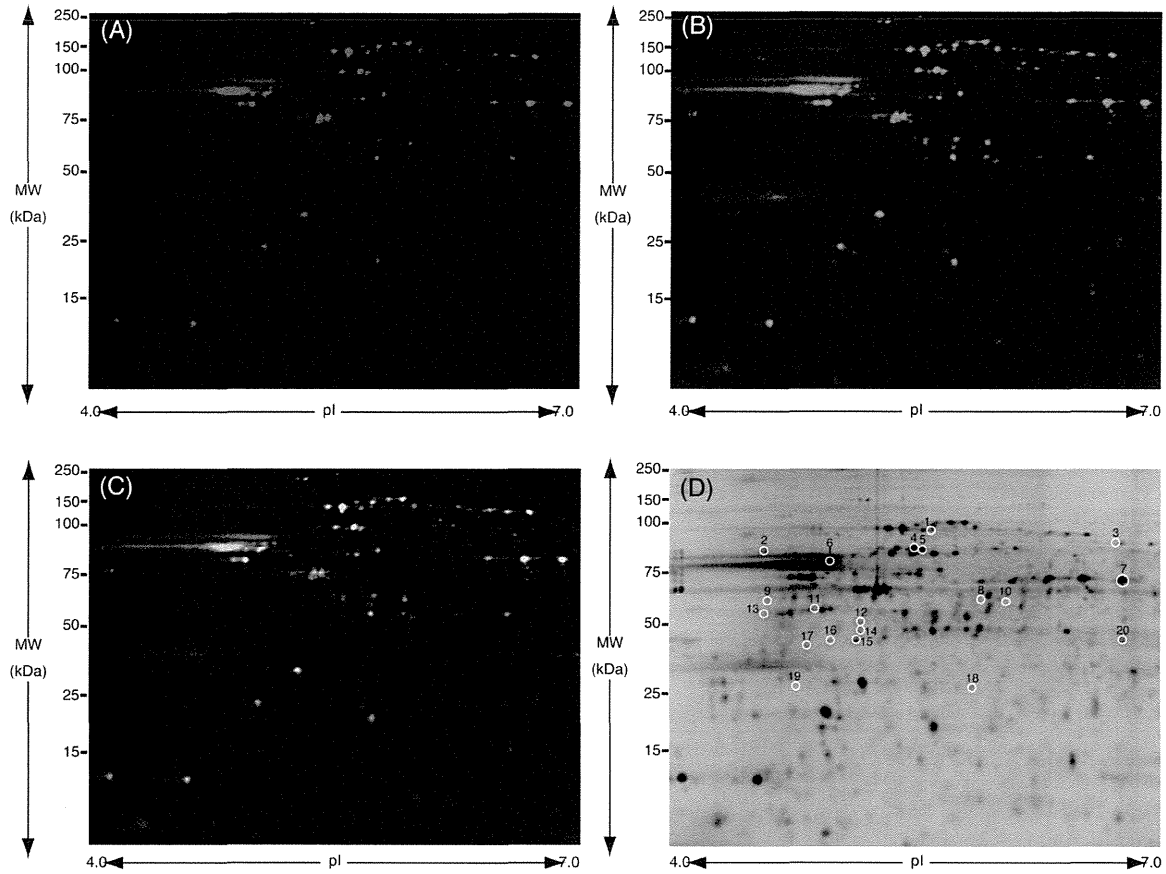

Fig. 1. 2D-DIGE gel image of fluorescence-labeled hippocampal proteins of non-transgenic and $APP_{E693\Delta}$-transgenic mice. (A) Analysis of the proteome of non-transgenic mice hippocampi with Cy3 Dye. (B) $APP_{E693\Delta}$-transgenic mice hippocampi with Cy5 Dye. (C) Merged. (D) Fourteen protein spots identified from non-transgenic and $APP_{E693\Delta}$-transgenic mice hippocampi by LC/MS/MS. Black numbers with white circles indicate proteins that are listed in Table 1.

Cy3 (Fig. 1A) and one replicate with Cy5 (Fig. 1B), resulting in three analytical gels. The 2D-DIGE comparative analysis of the wild type and $APP_{E693\Delta}$-transgenic mice revealed significant 74 spots (Fig. 1C). These spots were investigated by LC–MS/MS (Fig. 1D). Finally, fourteen proteins were identified as shown in Table 1. These proteins are classified into several groups that are involved in cytoskeletal, chaperone, energy metabolic, vesicle transport and signaling proteins (Table 2).

Spot nos. 1, 3 and 4 were identified as heat shock-related 70 kDa protein 2, stress-induced-phosphoprotein 1 and HSP60, respectively. The stress-induced-phosphoprotein 1 is the co-chaperone and thought of the function in regulation of interaction with Hsp70 and Hsp90 [10]. HSP60 is the chaperonin which is implicated in mitochondrial protein import and macromolecular assembly and may facilitate the correct folding of imported proteins [9]. The amounts of heat shock-related 70 kDa protein 2, stress-induced-phosphoprotein 1, and HSP60 were significantly decreased. On the contrary, spot no. 9 which was identified as heat shock cognate 71 kDa protein was significantly increased. This protein is also the chaperone and acts as a repressor of transcriptional activation [8]. Thus, Aβ oligomers might contribute to changing the expression of the chaperons.

Spot nos. 8, 10–12 and 16 were identified as actin, and spot nos. 15 and 17 were identified as tubulin β-2A chain. Actin is one of the major cytoskeletal proteins in neurons, and the dynamics of its assembly are involved in many aspects of cell motility, vesicle transport, and membrane turnover [14]. Actin itself is known to link with Aβ, which enhances the neurotoxicity induced by tau-mediated actin filament formation [4]. The four spots of actin but not no. 12 and those of tubulin were significantly increased. Thus, Aβ oligomers might lead to increasing the amounts of actin and tubulin.

Spot nos. 5 and 2 were identified as α-internexin and NFL, respectively, which are known as neuronal intermediate proteins [2,18]. The amounts of α-internexin and NFL were significantly decreased. Thus, the decreased amounts of NFL and internexin might raise neural dysfunction in the hippocampus of AD.

Spot nos. 7 and 13 were identified as α-enolase. Spot nos. 14 and 19 were identified as γ-enolase and ATP synthase subunit β, respectively. Enolase is a multifunctional protein as glycolytic enzyme, belonging to a novel class of surface proteins [11]. ATP synthase is a key role enzyme that provides energy for the cell to use through the synthesis of ATP [1]. The amount of α-enolase was significantly decreased, but the amounts of γ-enolase and ATP synthase subunit β were significantly increased. Interestingly, the levels of α-enolase and ATP synthase subunit α mitochondrial proteins significantly increased in the hippocampus of J20 Tg mice with amyloid deposition [19]. The amyloid deposit enhanced the expression of energy metabolic proteins [22]. Combined with our findings, both Aβ oligomers and amyloid deposition might play an important role in the change of energy metabolic proteins as α-enolase, γ-enolase and ATP synthase subunit β.

Spot no. 20 was identified as dynamin. Dynamin, a well studied neuron-specific mechanochemical GTPase, pinches off synaptic vesicles, freeing them from the membrane and allowing them to re-enter the synaptic vesicle pool to be refilled for future release

Table 1
Identified proteins from differentially expressed in the hippocampus of$APP_{E693\Delta}$-transgenic mice when compared to non-transgenic littermates.

Spot no.	Protein ID	Fold (APP/WT)	*t*-Test	Accession	Coverage	#Peptides	Predicted MW (kDa)	Calc. pI	Score
1	Heat shock-related 70 kDa protein 2	−1.32	0.040	P14659	26.22	23	69.6	5.67	625.70
2	Neurofilament light polypeptide	−1.48	0.002	P08551	39.96	43	61.5	4.64	1004.84
3	Stress-induced-phosphoprotein 1	−1.44	0.002	Q60864	16.21	9	62.5	6.80	157.49
4	60 kDa heat shock protein	−1.36	0.013	P63038	52.71	71	60.9	6.18	1916.39
5	Alpha-internexin	−1.34	0.023	P46660	42.66	39	55.7	5.27	1119.47
6	Protein kinase C and cascin kinase substrate in neurons protein 1	−1.48	0.023	Q61644	28.34	15	50.5	5.24	356.92
7	Alpha-enolase	−1.32	0.000	P17182	34.33	24	47.1	6.80	474.21
8	Actin, cytoplasmic 1	1.51	0.003	P60709	25.87	14	41.7	5.48	231.79
9	Heat shock cognate 71 kDa protein	1.35	0.015	P63017	12.54	16	70.8	5.52	319.85
10	Actin, cytoplasmic	1.34	0.004	P60709	24.27	13	41.7	5.48	279.37
11	Actin, cytoplasmic 1	1.38	0.022	P60709	15.47	7	41.7	5.48	243.14
12	Actin, cytoplasmic 1	−1.56	0.013	P60709	22.67	12	41.7	5.48	131.57
13	Gamma-enolase	1.33	0.005	P17183	20.05	13	47.3	5.11	237.25
14	ATP synthase subunit beta	1.40	0.047	P56480	23.60	18	56.3	5.34	356.19
15	Tubulin beta-2A chain	1.31	0.021	Q13885	14.83	13	49.9	4.89	313.07
16	Actin, cytoplasmic 1	1.47	0.002	P60709	6.93	3	41.7	5.48	97.01
17	Tubulin beta-2S chain	1.44	0.009	Q13885	11.46	5	49.9	4.89	118.50
18	Clathrin light chain B	1.68	0.005	P09497	8.30	3	25.2	4.64	95.06
19	ATP synthase subunit beta	1.46	0.013	P06576	16.64	16	56.5	5.40	283.06
20	Dynamin-1	1.40	0.006	Q05193	9.61	13	97.3	7.17	242.16

Mass spectrometry protein identification of 2D-DIGE spots of interest and statistical analysis using *t*-test between wild type mice and $APP_{E693\Delta}$-transgenic mice gels ($P < 0.05$). The proteins of mouse hippocampus were separated by 2DE and identified by LC MS/MS, following in-gel digestion with trypsin. The spots representing identified proteins are indicated in Fig. 1D and are designated with their ID accession numbers of Swiss Prot database. Score relates to the probability assignment. Score and sequence coverage were calculated by MASCOT search engine (http://www.matrixscience.com).

Table 2
Functions regulated by proteins that showed an altered expression in $APPE_{693\Delta}$-transgenic mouse hippocampus.

Function	Identified protein	Up/down
Cytoskeletal and their interacting proteins	Neurofilament light polypeptide	Down
	Alpha-internexin	Down
	Actin, cytoplasmic 1	Up/down
	Tubulin β-2A Chain	Up
Chaperone and their interacting proteins	Stress-induced-phosphoprotein 1	Down
	60 kDa heat shock protein	Down
	Heat shock cognate 71 kDa protein	Down
Energy metabolic proteins	Alpha-enolase	Down
	Gamma-enolase	Up
	ATP synthase subunit beta	Up
Vesicle transport and recycling	Dynamin-1	Up
	Clathrin light chain B	Up
Signaling proteins	Protein kinase C and casein kinase substrate in neurons protein 1	Down

The analysis of proteins function was done by using MOTIF (http://www.genome.jp/tools/motif/).

[12]. The amount of dynamin was significantly increased. Our findings in $APP_{E693\Delta}$-transgenic mice without plaque deposition are consistent with previous findings that protein levels of dynamin were increased in Tg2576 mice with plaque deposition [21], suggesting that the release of neurotransmitter is affected by dynamin increased irrespective of AD stage. Also, spot no. 6 was identified as Pacsin 1. The Pacsin 1 is colocalized, oligomerized and bound with dynamin, and both proteins participate in synaptic vesicle endocytosis [17]. The amount of Pacsin 1 was significantly increased. Taken together, Pacsin 1 and dynamin enhanced by Aβ oligomers

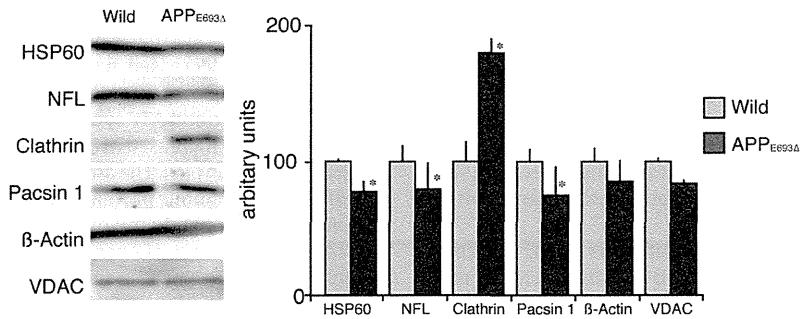

Fig. 2. Differentially expressed proteins validated by Western blotting for the hippocampus of non-transgenic and $APP_{E693\Delta}$-transgenic mice. (A) The levels of HSP60, NFL, clathrin, Pacsin 1, β-actin and VDAC in individual samples of each group were detected. (B) Graphical representation of the semi quantitative analysis (mean ± SEM of O.D. of bands). Data are presented as mean ± SEM ($n = 4$) *t*-test; $^*P < 0.05$ vs. $APP_{E693\Delta}$-transgenic mice.

might change the function of synaptic vesicle in the hippocampus of AD.

Spot no. 18 was identified as clathrin, which is known as the major protein of the polyhedral coat of coated pits and vesicles [7]. The amount of spot no. 18 was significantly decreased. APP was associated clusters of clathrin-coated vesicles and endosomes [3]. Thus, Aβ oligomers might inhibit the vesicle formation by clathrin.

In addition, we performed a validation experiment for HSP60, NFL, clathrin, Pacsin 1 and β-actin as the altered proteins, and VDAC as the unchanged protein (as control) [23]. The increased levels of clathrin, the decreased levels of HSP60, NFL, and Pacsin 1 and the unchanged level of β-actin and VDAC in $APP_{E693\Delta}$-transgenic mice hippocampus were validated by Western blotting (Fig. 2).

In summary, we identified the altered levels of 14 proteins in $APP_{E693\Delta}$-transgenic mice hippocampus using 2D-DIGE and LC–MS/MS approach. This approach elucidated the pathological effects of Aβ oligomers on hippocampus. Our findings might provide a clue for investigation of the hippocampus of AD early stage.

Acknowledgements

This work was supported by grants from Kobe Gakuin University for Collaborative Research C and the Smoking Research Foundation. The authors thank Dr. Tadanori Mayumi for his encouragement during the early days of the study.

References

[1] U. Andersson, H. Antonicka, J. Houstek, B. Cannon, A novel principle for conferring selectivity to poly(A)-binding proteins: interdependence of two ATP synthase beta-subunit mRNA-binding proteins, Biochemical Journal 346 (Pt 1) (2000) 33–39.
[2] C.L. Chien, R.K. Liem, Characterization of the mouse gene encoding the neuronal intermediate filament protein alpha-internexin, Gene 149 (1994) 289–292.
[3] A. Ferreira, A. Caceres, K.S. Kosik, Intraneuronal compartments of the amyloid precursor protein, Journal of Neuroscience 13 (1993) 3112–3123.
[4] T.A. Fulga, I. Elson-Schwab, V. Khurana, M.L. Steinhilb, T.L. Spires, B.T. Hyman, M.B. Feany, Abnormal bundling and accumulation of F-actin mediates tau-induced neuronal degeneration in vivo, Nature Cell Biology 9 (2007) 139–148.
[5] A. Gorg, C. Obermaier, G. Boguth, A. Harder, B. Scheibe, R. Wildgruber, W. Weiss, The current state of two-dimensional electrophoresis with immobilized pH gradients, Electrophoresis 21 (2000) 1037–1053.
[6] J. Hardy, D.J. Selkoe, The amyloid hypothesis of Alzheimer's disease: progress and problems on the road to therapeutics, Science 297 (2002) 353–356.
[7] J. Hirst, M.S. Robinson, Clathrin and adaptors, Biochimica et Biophysica Acta 1404 (1998) 173–193.
[8] C.R. Hunt, A.J. Parsian, P.C. Goswami, C.A. Kozak, Characterization and expression of the mouse Hsc70 gene, Biochimica et Biophysica Acta 1444 (1999) 315–325.
[9] S. Ikawa, R.A. Weinberg, An interaction between p21ras and heat shock protein hsp60, a chaperonin, Proceedings of the National Academy of Sciences 89 (1992) 2012–2016.
[10] J.L. Johnson, A. Halas, G. Flom, Nucleotide-dependent interaction of Saccharomyces cerevisiae Hsp90 with the cochaperone proteins Sti1, Cpr6, and Sba1, Molecular and Cellular Biology 27 (2007) 768–776.
[11] M. Kaghad, X. Dumont, P. Chalon, J.M. Lelias, N. Lamande, M. Lucas, M. Lazar, D. Caput, Nucleotide sequences of cDNAs alpha and gamma enolase mRNAs from mouse brain, Nucleic Acids Research 18 (1990) 3638.
[12] B.L. Kelly, R. Vassar, A. Ferreira, Beta-amyloid-induced dynamin 1 depletion in hippocampal neurons. A potential mechanism for early cognitive decline in Alzheimer disease, Journal of Biological Chemistry 280 (2005) 31746–31753.
[13] W.L. Klein, G.A. Krafft, C.E. Finch, Targeting small Abeta oligomers: the solution to an Alzheimer's disease conundrum? Trends in Neurosciences 24 (2001) 219–224.
[14] T.B. Kuhn, P.J. Meberg, M.D. Brown, B.W. Bernstein, L.S. Minamide, J.R. Jensen, K. Okada, E.A. Soda, J.R. Bamburg, Regulating actin dynamics in neuronal growth cones by ADF/cofilin and rho family GTPases, Journal of Neurobiology 44 (2000) 126–144.
[15] V.M. Lee, M. Goedert, J.Q. Trojanowski, Neurodegenerative tauopathies, Annual Review of Neuroscience 24 (2001) 1121–1159.
[16] S. Li, S. Hong, N.E. Shepardson, D.M. Walsh, G.M. Shankar, D. Selkoe, Soluble oligomers of amyloid Beta protein facilitate hippocampal long-term depression by disrupting neuronal glutamate uptake, Neuron 62 (2009) 788–801.
[17] J. Modregger, B. Ritter, B. Witter, M. Paulsson, M. Plomann, All three PACSIN isoforms bind to endocytic proteins and inhibit endocytosis, Journal of Cell Science 113 (Pt 24) (2000) 4511–4521.
[18] R.A. Nixon, R.K. Sihag, Neurofilament phosphorylation: a new look at regulation and function, Trends in Neurosciences 14 (1991) 501–506.
[19] R.A. Robinson, M.B. Lange, R. Sultana, V. Galvan, J. Fombonne, O. Gorostiza, J. Zhang, G. Warrier, J. Cai, W.M. Pierce, D.E. Bredesen, D.A. Butterfield, Differential expression and redox proteomics analyses of an Alzheimer disease transgenic mouse model: effects of the amyloid-beta peptide of amyloid precursor protein, Neuroscience 177 (2011) 207–222.
[20] D.J. Selkoe, Alzheimer's disease is a synaptic failure, Science 298 (2002) 789–791.
[21] S.J. Shin, S.E. Lee, J.H. Boo, M. Kim, Y.D. Yoon, S.I. Kim, I. Mook-Jung, Profiling proteins related to amyloid deposited brain of Tg2576 mice, Proteomics 4 (2004) 3359–3368.
[22] R. Sultana, D. Boyd-Kimball, J. Cai, W.M. Pierce, J.B. Klein, M. Merchant, D.A. Butterfield, Proteomics analysis of the Alzheimer's disease hippocampal proteome, Journal of Alzheimer's Disease 11 (2007) 153–164.
[23] M. Takano, K. Maekura, M. Otani, K. Sano, T. Nakamura-Hirota, S. Tokuyama, K.S. Min, T. Tomiyama, H. Mori, S. Matsuyama, Proteomic analysis of the brain tissues from a transgenic mouse model of amyloid beta oligomers, Neurochemistry International 61 (2012) 347–355.
[24] M. Takano, M. Otani, A. Sakai, K. Kadoyama, S. Matsuyama, A. Matsumoto, M. Takenokuchi, M. Sumida, T. Taniguchi, Use of a phosphosensor dye in proteomic analysis of human mutant tau transgenic mice, Neuroreport 20 (2009) 1648–1653.
[25] T. Tomiyama, S. Matsuyama, H. Iso, T. Umeda, H. Takuma, K. Ohnishi, K. Ishibashi, R. Teraoka, N. Sakama, T. Yamashita, K. Nishitsuji, K. Ito, H. Shimada, M.P. Lambert, W.L. Klein, H. Mori, A mouse model of amyloid beta oligomers: their contribution to synaptic alteration, abnormal tau phosphorylation, glial activation, and neuronal loss in vivo, Journal of Neuroscience 30 (2010) 4845–4856.

blood

2013 121: 2804-2813
Prepublished online January 30, 2013;
doi:10.1182/blood-2012-12-468363

Robo4 is an effective tumor endothelial marker for antibody-drug conjugates based on the rapid isolation of the anti-Robo4 cell-internalizing antibody

Mai Yoshikawa, Yohei Mukai, Yoshiaki Okada, Yuki Tsumori, Shin-ichi Tsunoda, Yasuo Tsutsumi, William C. Aird, Yasuo Yoshioka, Naoki Okada, Takefumi Doi and Shinsaku Nakagawa

Blood (print ISSN 0006-4971, online ISSN 1528-0020), is published weekly by the American Society of Hematology, 2021 L St, NW, Suite 900, Washington DC 20036.

Regular Article

VASCULAR BIOLOGY

Robo4 is an effective tumor endothelial marker for antibody-drug conjugates based on the rapid isolation of the anti-Robo4 cell-internalizing antibody

Mai Yoshikawa,[1] Yohei Mukai,[1,2] Yoshiaki Okada,[1] Yuki Tsumori,[1] Shin-ichi Tsunoda,[2] Yasuo Tsutsumi,[1,2] William C. Aird,[3] Yasuo Yoshioka,[1] Naoki Okada,[1] Takefumi Doi,[1] and Shinsaku Nakagawa[1]

[1]Graduate School of Pharmaceutical Sciences, Osaka University, Osaka, Japan, [2]Laboratory of Biopharmaceutical Research, National Institute of Biomedical Innovation (NiBio), Osaka, Japan, [3]Center for Vascular Biology Research and Division of Molecular and Vascular Medicine, Beth Israel Deaconess Medical Center, Boston, MA

Key Points

- First therapeutic application that targets Robo4 on the tumor blood vasculature
- High-throughput screening system to isolate cell-internalizing monoclonal antibodies useful to develop effective antibody-drug conjugates

Monoclonal antibodies (mAbs) that are internalized into cells are a current focus in the development of antibody-drug conjugates (ADCs). We describe a phage display–based high-throughput screening system to rapidly isolate cell-internalizing mAbs. We simultaneously examined the cell-internalizing activities of several hundred independent mAbs and successfully isolated cell-internalizing mAbs against the tumor endothelial markers Roundabout homolog 4 (Robo4) and vascular endothelial growth factor receptor 2 (VEGFR2). Tumor accumulation of mAbs with high cell-internalizing activity was significantly higher than that of mAbs with low cell-internalizing activity. Furthermore, the antitumor effects of ADCs of mAbs with high cell-internalizing activity were significantly stronger than those of mAbs with low cell-internalizing activity. Although anti-VEGFR2 therapy caused a significant loss of body weight, anti-Robo4 therapy did not. These findings indicate that cell-internalizing activity plays an important role in the biodistribution and therapeutic effects of ADCs. Further, Robo4 can be an effective marker for tumor vascular targeting. (*Blood.* 2013;121 (14):2804-2813)

Introduction

Antibody drug conjugates (ADCs), ie, monoclonal antibodies (mAbs) labeled with certain anticancer agents, are currently the focus of antibody-based drug discovery. ADCs have mAb-derived specificity and allow for targeted delivery of cytotoxic drugs to a tumor, which is expected to significantly enhance the antitumor activity of mAbs.[1] Trastuzumab ematansine (T-DM1)[2] for human epidermal growth factor receptor 2 (Her-2)–positive breast cancer and brentuximab vedotin (SGN-35)[3] for relapsed or refractory CD30-positive lymphoproliferative disorders are now in phase 3 clinical trials as effective ADCs.[4] ADCs will have an important role in overcoming some types of refractory cancers and will contribute to the field of tumor vascular targeting.[5]

An essential property of ADCs is that the mAb should be efficiently internalized into the cell where the cytotoxic effects of anticancer drugs occur.[1] The isolation of mAbs with high cell-internalizing activity (cell-internalizing mAbs) is a limiting factor in the development of ADCs. The discovery of potent cell-internalizing mAbs, however, requires labor-intensive screening of a massive number of candidates, and therefore the development of phage display–based methods to identify these candidates is highly desirable.[6,7] In the phage display–based method, a phage antibody library is added to the desired cells and then phages bound to the cell surface are removed. Only internalized phages are rescued from the intracellular compartment. Even with this method, however, the internalizing activities of individual antibody candidates must be assessed, because the concentrated phage pool comprises a "polyclonal" population. To address this issue, we used high-throughput screening methods to estimate "monoclonal" cell-internalization activities using a protein synthesis inhibitory factor (PSIF),[8] which provided a breakthrough in reducing the time-consuming screening of the cell-internalizing activity.

PSIF is a fragment of a bacterial exotoxin derived from *Pseudomonas aeruginosa*.[9] PSIF lacks its cell binding domain, and its cytotoxic portion is used in a recombinant immunotoxin.[10] Upon entry into the cell, PSIF has strong cytotoxicity by inducing ADP-ribosylation of elongation factor-2, which is essential for protein synthesis.[11] Our group previously accelerated the identification of cell-internalizing novel protein transduction domains (PTDs) by expressing PTD-PSIF fusion proteins in the supernatant of *Escherichia coli*.[8] Using this system, we successfully discovered superior HIV-Tat PTD mutants by simultaneously estimating

Submitted December 3, 2012; accepted January 22, 2013. Prepublished online as *Blood* First Edition paper, January 30, 2013; DOI 10.1182/blood-2012-12-468363.

M.Y. and Y.M. contributed equally to this study.

The online version of this article contains a data supplement.

The publication costs of this article were defrayed in part by page charge payment. Therefore, and solely to indicate this fact, this article is hereby marked "advertisement" in accordance with 18 USC section 1734.

the cell-internalizing activities of several hundred monoclonal PTD-PSIF fusions.[8] Therefore, we expect this method to contribute to the identification of mAbs with high cell-internalizing activity (cell-internalizing mAbs) by expressing single-chain antibody Fv (scFv)-PSIF fusion proteins to estimate the cell-internalizing activities of a very large number of antibodies.

Roundabout homolog 4 (Robo4) is a potential tumor angiogenesis marker.[12] Robo4 expression is restricted to areas of in vivo angiogenesis[13,14] and the subpopulation of hematopoietic stem cells localized in the bone marrow.[15] At angiogenic sites, Robo4 is present in the endothelial lining of blood vessels in the developing embryo,[16] placenta,[14] and tumors.[17] We previously confirmed the endothelial cell–specific expression of Robo4 using transgenic mouse lines.[18,19] Robo4 acts as a receptor that modulates vascular endothelial growth factor A (VEGF)–VEGF receptor (VEGFR) signaling.[20-23] Therefore, Robo4 is a potential marker for tumor vascular targeting because angiogenesis is only activated in tumors in the adult,[24] with the exception of some pathological states.[25,26] Another potential tumor angiogenesis marker is VEGFR2, a well-established tumor endothelial marker.[27] The VEGF-VEGFR2 signaling pathway plays a crucial role in angiogenesis, and anti-VEGF mAbs and small molecule inhibitors against VEGFR are approved for various types of cancers.[28] Anti-VEGFR2 mAbs are also used for tumor vascular targeting.[29] Although VEGFR2 is strongly expressed in active angiogenic sites, its expression is also observed in normal tissues.[30] Hypertension and proteinuria are common side effects of anti-VEGF therapy because VEGF-VEGFR signaling is also inhibited in normal tissue, including the kidney, heart, and resistance vessels.[31-33]

Here we applied the PSIF system to search for novel cell-internalizing mAbs from an immune phage antibody library. Application of this method to Robo4 and VEGFR2 led to the successful discovery of anti-Robo4 and anti-VEGFR2 cell-internalizing mAbs, as well as mAbs with low cell-internalizing activity (low-internalizing mAbs) to be used as controls. Comparing mAbs with different cell-internalizing activities revealed that higher cell-internalizing activity enhanced the tumor targeting potency of mAbs. Furthermore, comparative studies with anti-Robo4 and anti-VEGFR2 cell-internalizing mAbs in vivo indicated that Robo4 was superior to VEGFR2 in terms of the therapeutic window. This is the first report demonstrating the benefits of cell-internalizing mAbs in tumor vascular targeting. Further, these findings demonstrate the potential of Robo4 as a target for further development of novel ADCs against tumor blood vasculature.

Materials and methods

Cell culture

MS1 immortalized murine endothelial cells were cultured in Dulbecco's Modified Eagle Medium containing 5% fetal bovine serum 1% antibiotic-antimycotic mixed solution. B16BL6 murine melanoma cells were cultured in minimum essential medium containing 10% fetal bovine serum and 1% antibiotic-antimycotic mixed solution at 37°C. These cells were maintained at 37°C under a humidified 5% CO_2 atmosphere.

B16BL6 tumor-bearing mice

B16BL6 cells (1×10^6 cells/100 μL) were inoculated intracutaneously into 6-week-old female C57BL6 mice (Japan SLC Inc., Shizuoka, Japan) (day 0). Biodistribution was analyzed on the day that the tumor width reached 10 mm. The therapy experiment was started on day 3. As a validation of the model, we confirmed the expressions of VEGFR2 and Robo4 on the tumor endothelium, based on the immunofluorescence against B16BL6 tumor sections.

Antigens

Human VEGFR2 (hVEGFR2) and mouse VEGFR2 (mVEGFR2) were commercial recombinant proteins (Merck Chemicals, Inc., Darmstadt, Germany, or R&D Systems, Inc., Minneapolis, MN). Human Robo4 (hRobo4) and mouse Robo4 (mRobo4) were produced as described previously.[34]

Immune phage antibody libraries

Phage antibody libraries were constructed from the spleen and bone marrow cells of immunized mice as previously described.[35,36] Our phage antibody library comprised single-chain Fv fragment (scFv) fused with pIII phage coat protein. Four rounds of affinity panning were performed against hVEGFR2 and mVEGFR2 for the anti-VEGFR2 immune library, and against hRobo4 and mRobo4 for the anti-Robo4 immune library. Anti-FLAG panning was followed by each panning to concentrate the scFv-displaying phages, as described previously.[36]

ELISA and cytotoxicity assay using TG1 supernatant

Plasmids were extracted from TG1 cells after the fourth panning against mVEGFR2 or mRobo4. These "enriched" scFv gene libraries were cloned into a PSIF-fusion expression vector derived from pCANTAB5E.[8] Monoclonal scFv-PSIF protein was induced in the TG1 supernatant, as previously described.[8] mVEGFR2 or mRobo4 was immobilized on an immunoassay plate and blocked with 4% skim milk in phosphate-buffered saline (PBS) (4% MPBS) at 37°C for 2 hours. TG1 supernatant containing 2% MPBS was reacted with antigens at room temperature for 1 hour. Bound scFv-PSIFs were detected by anti–FLAG-horseradish peroxidase (M2, Sigma-Aldrich Corporation, St. Louis, MO). For the cytotoxicity assay, MS1 cells were seeded on a 96-well plate at 1.0×10^4 cells/well. After incubation at 37°C for 24 hours, TG1 supernatant was diluted in MS1 culture medium, and then added to the MS1 cells. After incubation at 37°C for 24 hours, cell viability was assessed using a WST-8 assay (Dojindo Molecular Technologies, Inc., Kumamoto, Japan). The viability of nontreated MS1 and completely killed MS1 with 1 mM cycloheximide were defined as 100% and 0%, respectively.

Expression and purification of scFv, dscFv, and scFv-PSIF recombinant protein

The isolated scFv gene with 15 amino acids linker (VL-GGGGSGGG GSGGGGS-VH) was cloned into modified pET15b vector, resulting in the scFv fused by FLAG-tag and His×6 tag at the C-terminus. A scFv gene with a 5–amino acid linker (VL-GGGGS-VH) was also cloned into modified pET15b, resulting in a noncovalent scFv dimer (dscFv) fused by FLAG-tag and His×6 tag at the C-terminus. An anti-His scFv gene was also cloned but only a FLAG-tag was fused at the C-terminus. A scFv gene with a 15–amino acid linker was cloned into pYas-PSIF vectors.[37] ScFvs, dscFvs, and scFv-PSIFs were purified from inclusion bodies in *E coli* according to the previously described methods.[37] The binding affinity of each recombinant protein was assessed by surface plasmon resonance using BIAcore3000 (GE Healthcare UK Ltd., Chalfont, United Kingdom).

Expression and purification of IgG recombinant protein

IgG recombinant proteins were expressed using an OptiCHO antibody expression kit (Invitrogen Corporation, Carlsbad, CA) according to the manufacturer's instructions. IgGs were purified from cell culture supernatant with protein G column (GE Healthcare). Eluted fractions were further purified with Superdex 200 column (GE Healthcare). Anti-FLAG[IgG] (anti-FLAG M2 antibody) was purchased from Sigma-Aldrich.

Preparation of IgG-NCS

NCS was kindly provided by Kayaku Co, Ltd., Tokyo, Japan. NCS was thiolated by incubating it with 10 molar excess 2-iminothiolane (Thermo Fisher Scientific Inc., Waltham, MA) for 1 hour at room temperature. IgG recombinant proteins were reacted with 10 molar excess of SPDP

crosslinker (*N*-succinimidyl 3-[2-pyridyldithio]-propionate; Thermo Fisher) for 30 minutes on ice. SPDP-modified IgGs and thiolated NCS were separately purified using NICK columns (GE Healthcare). They were then mixed for 8 hours at room temperature. IgG-NCS were purified with a Superdex 200 column. Modification efficiency was quantified after sodium-dodecyl sulfate-polyacrylamide gel electrophoresis using a Gel DOC EZ system and Image laboratory software (Bio-Rad Laboratories, Inc., Hercules, CA).

Labeling of purified mAbs

For fluorescent labeling, mAbs were labeled using Cy5.5-NHS (GE Healthcare). For ^{125}I labeling, 100 μg mAbs in 0.4 M phosphate buffer were labeled with 0.2 mCi Na^{125}I (PerkinElmer, Inc., Waltham, MA) based on the chloramine-T method.[38] For biotin labeling, mAbs were biotinylated using EZ-Link Sulfo-NHS-Biotin (Thermo Fisher). Each mAb was purified using a NICK desalting column (GE Healthcare).

Flow cytometry

Cy5.5-labeled mAb (mAb$^{Cy5.5}$; 4 μM) was incubated with 5.0×10^5 cells of MS1 cells in 6-well plates for 2 hours at 4°C. After washing three times, the cells were incubated for an additional 0.5 to 8 hours at 37°C. At each time point, cells were collected in 2-mM ethylenediaminetetraacedtic acid/PBS. Bound mAbs were digested using 0.1% trypsin/PBS at 37°C for 20 minutes (trypsinized group) or PBS (nontrypsinized group). Cellular fluorescence was measured by Gallios flow cytometer (Beckman Coulter, Inc., Miami, FL). The ratio of internalization was calculated using the following formula: internalization (%) = {internalized mAb$^{Cy5.5}$}/{total bound mAb$^{Cy5.5}$} × 100 (%) = {(MFI of mAb)$_T$ − (MFI of anti-His [mAb])$_T$}/{(MFI of mAb)$_N$ − (MFI of anti-His[mAb])$_N$} × 100 (%). MFI indicates mean fluorescence intensity. T and N indicate trypsinized and nontrypsinized groups, respectively.

In vivo biodistribution

dscFvs^{125I} (0.2 nmol) was intravenously injected into B16BL6 tumor–bearing mice. At 2 hours and 24 hours after injection, the radioactivity of each organ was counted using the Wizard 2480 γ-ray counter (PerkinElmer). %ID/g tissue was calculated using following formula: %ID/g tissue = (count/g tissue)/(total injected count) × 100 (%). Two individual experiments were combined for the final data (total 11 mice/group).

Immunofluorescence of the tissue sections

B16BL6 tumor–bearing mice were administered 2 nmol of dscFvs^{Bio}. At 2 hours after the injection, the tumors, kidneys, and hearts were embedded in optimal cutting temperature compound (Sakura Finetek, Inc., Torrance, CA) and frozen in liquid nitrogen. Thin sections (7 μm) were prepared using a Cryostat CM1850 (Leica Microsystems GmbH, Wetzlar, Germany) and fixed in 4% paraformaldehyde. DscFvs^{Bio} in the sections were stained with streptavidin phycoerythrin conjugate (eBioscience Inc., San Diego, CA) in Dako REAL Antibody Diluent (DAKO Corporation, Carpinteria, CA). CD31+ vascular endothelial cells were stained with rat anti-CD31 antibody (MEC13.3; Becton Dickinson and Company, Franklin Lakes, NJ) in Dako REAL Antibody Diluent and Alexa488 conjugated anti-rat IgG (A11006; Invitrogen). The samples were embedded with Prolong Gold antifade reagent with 4′,6-diamidino-2-phenylindole (Invitrogen) and observed with a fluorescence microscope FSX100 (Olympus Corporation, Tokyo, Japan).

In vivo therapy experiments

Activities of scFv-PSIFs and IgG-NCSes were confirmed by WST-8 assay as described before. B16BL6 cells were inoculated intracutaneously into C57BL6 mice (Japan SLC) on day 0. Mice were intravenously injected with 15 pmol scFv-PSIFs and 10 pmol IgG-NCSs on days 3, 5, 7, 9, and 11 (7 mice/group). The volume of the tumor was calculated according to the following formula: tumor volume (mm^3) = {major axis of tumor (mm)} × {minor axis of tumor (mm)}^{2} × 0.4.

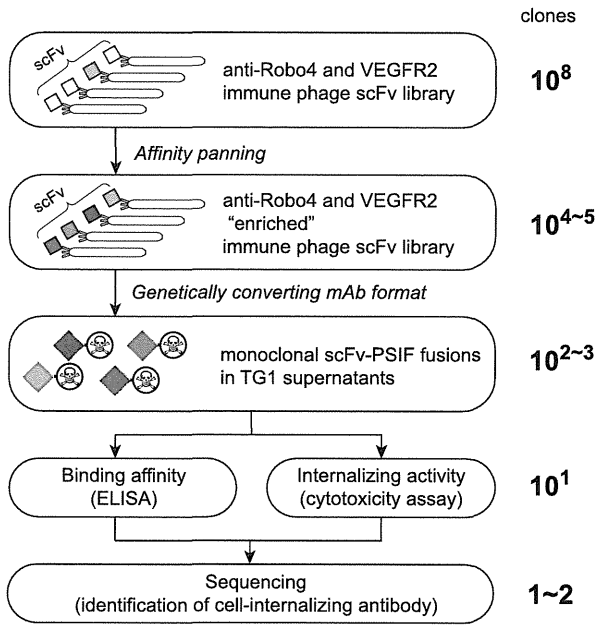

Figure 1. Phage display-based method to search for cell-internalizing mAbs. The phage antibody library was "enriched" by affinity panning against the desired antigens. Plasmids encoding scFvs were collected from TG1 *E coli* strains infected by "enriched" phage libraries. Genes of scFvs were digested out and ligated into a PSIF fusion protein expression vector. These plasmids were then transformed to TG1, and then single colonies were picked up. From these individual colonies, monoclonal scFv-PSIF fusions were induced in TG1 supernatants. Using these fusion proteins, binding affinities and internalizing activities of several hundreds of scFv-PSIFs were easily estimated by ELISA and cytotoxicity assays, respectively. Finally, genes of positive scFvs were collected from TG1, and cell-internalizing scFvs were identified by sequencing. In this report, we used anti-Robo4 and anti-VEGFR2 immune phage scFv libraries as the phage antibody libraries, and mRobo4 and mVEGFR2 as the desired antigens.

Results

High-throughput screening for cell-internalizing mAbs

To identify cell-internalizing mAbs, we applied the phage immune scFv library to high-throughput screening of cell-internalizing molecules based on the PSIF system[8] (Figure 1). Our anti-Robo4 or anti-VEGFR2 phage library comprised approximately 3.0×10^8 or 5.0×10^8 independent scFvs, which was validated by sequence analysis. To assess the qualities of the libraries, affinity panning was performed against each antigen. During the panning, output phages were increased, suggesting that the desired scFvs were enriched in the library (supplemental Figure 1A-B,E-F). After the fourth panning, >40% of monoclonal scFvs showed specific binding in enzyme-linked immunosorbent assay (ELISA) (supplemental Figure 1C-D,G-H).

To validate the efficacy of cell-internalizing mAbs in a mouse model, we selected libraries enriched against murine antigens (mRobo4 and mVEGFR2) and chose MS1 murine endothelial cells for the screening of cell-internalizing mAbs because we confirmed the expressions of both mRobo4 and mVEGFR2 in MS1 cells using reverse transcriptase–polymerase chain reactioin. For the screening, scFv genes obtained after the fourth round of panning were cloned into the PSIF expression vector. Monoclonal scFv-PSIFs were expressed in TG1 supernatants (315 clones per library). For anti-Robo4s, 178 of 315 clones bound to mRobo4 in ELISA and 20 of these 178 binders were cytotoxic against MS1 cells

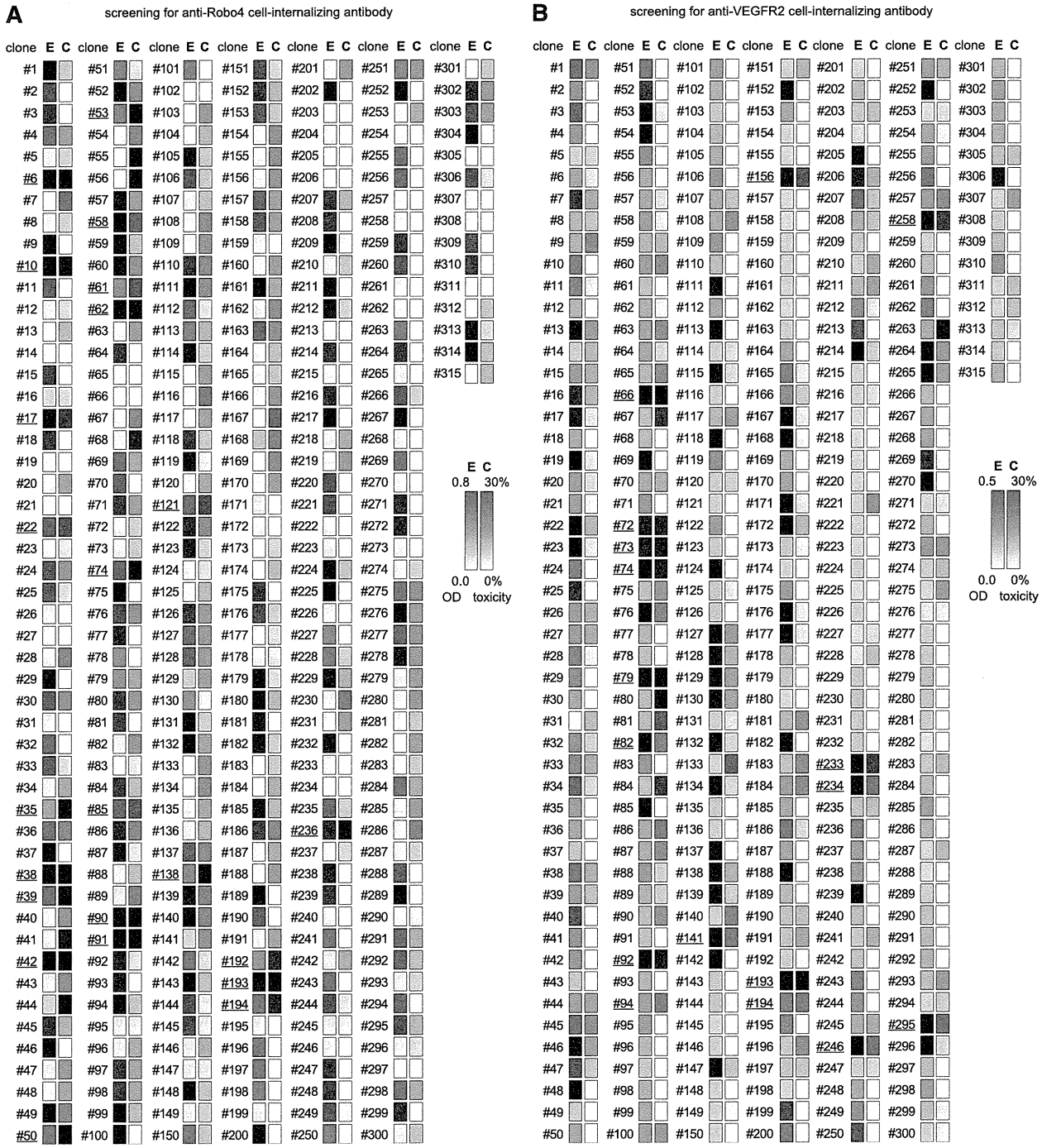

Figure 2. Screening of cell-internalizing mAbs (ELISA and cytotoxicity assay). To screen for cell-internalizing mAbs, 315 clones per antigen were analyzed by ELISA and cytotoxicity assay. (A) Result for Robo4, (B) Result for VEGFR2. Monoclonal scfv-PSIFs were induced in TG1 supernatant. The binding properties and cytotoxicities to MS1 cells were then assessed by an ELISA and WST-8 assay, respectively. E, ELISA results; C, WST-8 assay results. Individual results from ELISA (OD = 0.8 or 0.5~0.0) and WST-8 assay (cytotoxicity = 30%~0%) were mapped in grayscale densities. The 24 candidates against Robo4 and 17 candidates against VEGFR2 are indicated by the underline (ELISA OD ≥0.2 and cytotoxicity ≥20%). After omitting redundant clones by sequencing, 1 cell-internalizing mAb and 2 low-internalizing mAbs against mRobo4, and 2 cell-internalizing mAbs and 14 low-internalizing mAbs against mVEGFR2 were identified.

(Figure 2A). In a similar manner, for anti-VEGFR2s, 156 of 315 clones bound to VEGFR2 and 17 of the 156 binders were positive in the ELISA and cytotoxicity assays (Figure 2B). Sequence analysis to omit redundant clones revealed that these clones comprised 1 anti-Robo4 cell-internalizing mAb, 2 anti-Robo4 low-internalizing mAbs, 2 anti-VEGFR2 cell-internalizing mAbs, and 14 anti-VEGFR2 low-internalizing mAbs. For anti-Robo4s, only one anti-Robo4 cell-internalizing mAb was named "R4-13i" and a low-internalizing mAb with high affinity and low cytotoxicity was named "R4-16." In a similar manner, "V2-05i" and "V2-02" were selected as an anti-VEGFR2 cell-internalizing mAb and a low-internalizing mAb, respectively. After purification of the recombinant proteins, both anti-Robo4 scFvs bound to hRobo4, similar to mRobo4. Conversely, anti-VEGFR2 scFvs bound to

Table 1. Binding kinetics of antibodies in surface plasmon resonance analysis

Antibody	Target	Format	k_a ($M^{-1}s^{-1}$)	k_d (s^{-1})	K_D (M)
R4-13i	mRobo4	scFv	$1.25 \pm 0.36 \times 10^5$	$5.82 \pm 0.95 \times 10^{-4}$	$5.03 \pm 1.95 \times 10^{-9}$
(internalizing)		dscFv	$1.15 \pm 0.34 \times 10^6$	$5.98 \pm 0.61 \times 10^{-4}$	$5.64 \pm 2.21 \times 10^{-10}$
		IgG	$1.14 \pm 0.55 \times 10^6$	$4.19 \pm 1.70 \times 10^{-4}$	$2.22 \pm 0.51 \times 10^{-10}$
		scFv-PSIF	$7.22 \pm 4.31 \times 10^4$	$4.28 \pm 1.60 \times 10^{-3}$	$6.47 \pm 1.61 \times 10^{-8}$
		IgG-NCS	$1.02 \pm 0.15 \times 10^6$	$4.66 \pm 0.86 \times 10^{-4}$	$4.59 \pm 0.74 \times 10^{-10}$
R4-16	mRobo4	scFv	$1.30 \pm 0.33 \times 10^5$	$5.82 \pm 1.50 \times 10^{-4}$	$4.77 \pm 1.96 \times 10^{-9}$
(low-internalizing)		dscFv	$1.12 \pm 0.03 \times 10^6$	$5.91 \pm 1.50 \times 10^{-4}$	$5.31 \pm 1.96 \times 10^{-10}$
		IgG	$1.06 \pm 0.24 \times 10^6$	$3.60 \pm 0.85 \times 10^{-4}$	$2.76 \pm 0.16 \times 10^{-10}$
		scFv-PSIF	$8.90 \pm 1.42 \times 10^4$	$6.10 \pm 2.45 \times 10^{-3}$	$7.24 \pm 3.74 \times 10^{-8}$
		IgG-NCS	$1.07 \pm 0.12 \times 10^6$	$3.93 \pm 0.54 \times 10^{-4}$	$3.72 \pm 0.89 \times 10^{-10}$
V2-05i	mVEGFR2	scFv	$9.66 \pm 3.57 \times 10^4$	$4.40 \pm 0.95 \times 10^{-4}$	$5.13 \pm 2.61 \times 10^{-9}$
(internalizing)		dscFv	$8.75 \pm 2.03 \times 10^5$	$5.59 \pm 2.57 \times 10^{-4}$	$6.16 \pm 1.47 \times 10^{-10}$
		IgG	$1.14 \pm 0.09 \times 10^6$	$3.21 \pm 0.35 \times 10^{-4}$	$2.84 \pm 0.52 \times 10^{-10}$
		scFv-PSIF	$9.57 \pm 0.84 \times 10^4$	$6.51 \pm 1.87 \times 10^{-3}$	$6.94 \pm 2.63 \times 10^{-8}$
		IgG-NCS	$0.96 \pm 0.06 \times 10^6$	$4.37 \pm 0.90 \times 10^{-4}$	$4.52 \pm 0.79 \times 10^{-10}$
V2-02	mVEGFR2	scFv	$7.94 \pm 1.24 \times 10^4$	$4.28 \pm 3.23 \times 10^{-4}$	$5.07 \pm 3.05 \times 10^{-9}$
(low-internalizing)		dscFv	$8.94 \pm 2.55 \times 10^5$	$5.57 \pm 1.25 \times 10^{-4}$	$6.60 \pm 2.39 \times 10^{-10}$
		IgG	$1.13 \pm 0.22 \times 10^6$	$3.25 \pm 1.10 \times 10^{-4}$	$2.90 \pm 0.98 \times 10^{-10}$
		scFv-PSIF	$9.84 \pm 1.52 \times 10^4$	$5.75 \pm 2.05 \times 10^{-3}$	$5.81 \pm 1.93 \times 10^{-8}$
		IgG-NCS	$1.08 \pm 0.08 \times 10^6$	$5.25 \pm 1.58 \times 10^{-4}$	$4.85 \pm 1.30 \times 10^{-10}$

Binding kinetics were analyzed against mRobo4 (R4-13i and R4-16) or mVEGFR2 (V2-05i and V2-02). Values are shown as means ± SD from three different preparations.

k_a, association rate constant ($M^{-1}s^{-1}$); k_d, dissociation rate constant (s^{-1}); K_D, equilibrium dissociation constant (k_d/k_a) (M).

mVEGFR2, but not to hVEGFR2. We also confirmed using competitive ELISA that the mAbs did not share their antigen-binding epitopes (supplemental Figure 2).

Characterization of mAbs

We purified scFvs, dimerized scFvs (dscFvs), IgGs, and scFv-PSIF as recombinant proteins. IgGs conjugated with neocarzinostatin (IgG-NCSes) were also prepared for in vivo experiments. NCSes were confirmed to be conjugated to IgG molecules in the purified IgG-NCS fraction, and the efficiencies of the NCS modifications were similar in all IgG-NCSes (1.6~1.8 NCSes per single IgG). Surface plasmon resonance analysis revealed that cell-internalizing mAbs and low-internalizing mAbs had similar affinities against antigens in all antibody forms (Table 1).

To quantify the internalization, flow cytometry analysis was performed with Cy5.5-labeled mAbs ($scFv^{Cy5.5}$, $dscFv^{Cy5.5}$, and $IgG^{Cy5.5}$; Figure 3A,C). After $mAbs^{Cy5.5}$ bound to the cell surface, internalization was induced by incubation at 37°C for 2 hours. By removing cell-surface $mAbs^{Cy5.5}$ with trypsinization, the internalized $mAbs^{Cy5.5}$ were quantified by flow cytometry. At 2 hours, approximately 30% of cell-internalizing mAbs remained after trypsinization, whereas most of the low-internalizing mAbs were degraded (Figure 3A,C). This result clearly suggested that the internalization efficiencies differed between cell-internalizing mAbs and low-internalizing mAbs, even among the three different mAb forms. In a similar manner, a time-shift analysis revealed that >40% of cell-internalizing mAbs were internalized after 8 hours of incubation (Figure 3B,D). These findings indicate that only cell-internalizing mAbs were efficiently internalized into the cells, although low-internalizing mAbs had affinities similar to those of cell-internalizing mAbs (Table 1).

Intracellular localization

The intracellular behaviors of cell-internalizing mAbs were analyzed with a confocal laser-scanning microscope. In MS1 cells, intracellular fluorescence derived from $scFv^{Cy5.5}$ was observed with cell-internalizing scFvs, but not with low-internalizing scFvs (supplemental Figure 3A,D,E,H). Fluorescence was suppressed, however, under the inhibition of energy-dependent endocytosis (supplemental Figure 3B-C,F-G). These results suggested that cell-internalizing scFvs entered into the cells via energy-dependent endocytosis.

For in-depth analysis of the intracellular behavior, confocal laser-scanning microscope analysis was performed with immunostaining of endosome markers (supplemental Figure 3Iab). After $scFvs^{Cy5.5}$ were bound to the cell-surface, the cells were incubated for an additional 1 to 8 hours at 37°C. The early endosome marker, early endosome antigen 1 (EEA1), and the late endosome marker, lysosomal-associated membrane protein 1 (LAMP1), were visualized using Alexa488-conjugated antibodies. Colocalization with EEA1+ early endosomes decreased over time (supplemental Figure 3I-M,S-W), whereas colocalization with LAMP1+ late endosomes increased (supplemental Figure 3N-R,Xab). These findings suggested that cell-internalizing scFvs were encapsulated in EEA1+ early endosomes at an early stage and eventually accumulated in LAMP1+ late endosomes. This is thought to be a typical endocytotic molecular sorting pathway.[39]

Influence of cell-internalizing activity on biodistribution

To assess the biodistribution of cell-internalizing mAbs, ^{125}I-labeled dscFvs ($dscFv^{125I}$) were intravenously injected into B16BL6 tumor-bearing mice. In this experiment, we selected the dscFv form because dscFv has superior in vivo tumor-targeting potency compared with scFv.[40] At 2 hours, the tumor distribution of anti-Robo4 and anti-VEGFR2 $dscFvs^{125I}$ was similar to but significantly higher than that of a negative control $dscFv^{125I}$ ($anti\text{-}His[dscFv]^{125I}$; Figure 4A-B). This finding suggested that the anti-Robo4 and anti-VEGFR2 dscFvs had tumor-targeting properties. Anti-Robo4 $dscFvs^{125I}$ also accumulated in the kidney, indicating a nonspecific distribution of dscFvs for their elimination,[41,42] because no significant difference was observed between anti-Robo4 $dscFvs^{125I}$

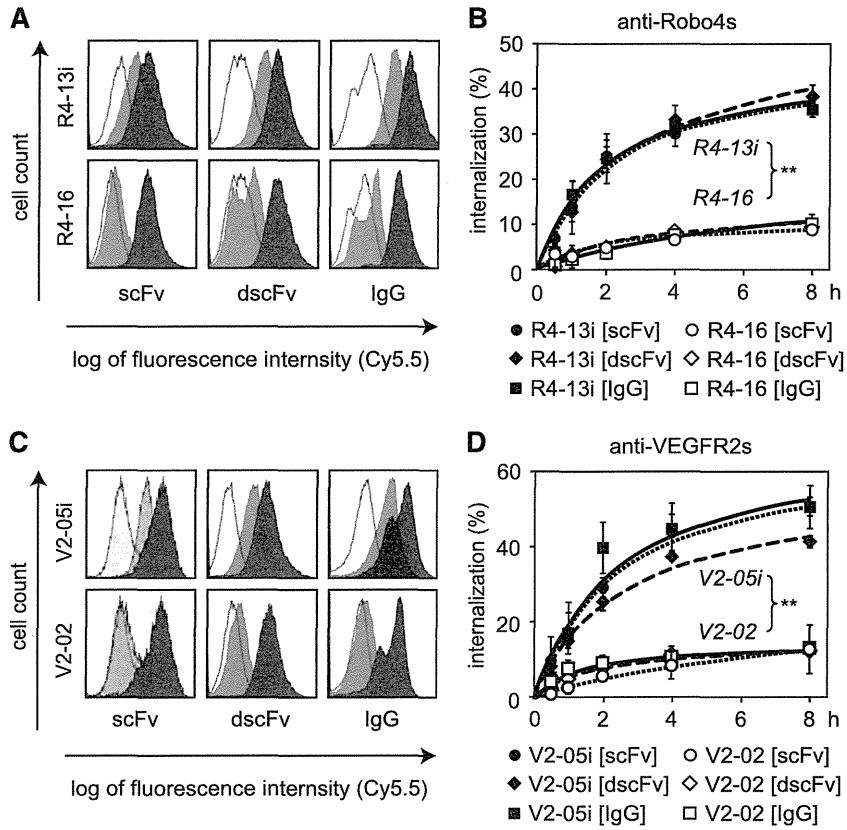

Figure 3. Cell internalization analyzed by flow cytometry. (A,C) Trypsinization to quantify internalized mAbs. Different forms of $mAbs^{Cy5.5}$ bound to the MS1 cells at 4°C. After washing out the unbound mAbs, internalization was induced for 2 hours at 37°C. To detect only internalized mAbs, cell surface proteins were trypsinized. The remaining cellular fluorescence was then analyzed by flow cytometry. (A) Anti-Robo4 $mAbs^{Cy5.5}$, (C) Anti-VEGFR2 $mAbs^{Cy5.5}$. Black, nontrypsinized group; gray, trypsinized group; white, negative control (anti-His[scFv]$^{Cy5.5}$, anti-His[dscFv]$^{Cy5.5}$, or anti-FLAG [IgG]$^{Cy5.5}$). (B,D) Time course of the internalization. After binding at 4°C, internalization was induced for 0.5, 1, 2, 4, or 8 hours at 37°C. The ratio of internalization was calculated using the following formula: internalization (%) = {internalized mAb}/{total bound mAb} × 100 (%) = {(MFI of $mAb)_T$ − (MFI of negative $control)_T$}/{(MFI of $mAb)_N$ − (MFI of negative $control)_N$} × 100 (%). T, trypsinized group; N, nontrypsinized group; MFI, mean fluorescence intensity. (B) Closed and open markers indicate R4-13i and R4-16, respectively. (D) Closed and open markers indicate V2-05i and V2-02, respectively. (B,D) Circles, diamonds, and squares indicate scFv, dscFv, and IgG, respectively. Each experiment was performed in triplicate. Values are shown as means ± SD. $^{**}P < .01$; internalizing mAb versus low-internalizing mAb in each form by 2-way ANOVA (n = 3).

and anti-His[dscFv]^{125I} (Figure 4A). Importantly, the accumulation of anti-VEGFR2 $dscFvs^{125I}$ in the kidney was significantly greater than that of anti-His[dscFv]^{125I} (Figure 4B). A similar accumulation of anti-VEGFR2 $dscFvs^{125I}$, but not anti-Robo4 $dscFvs^{125I}$ (Figure 4A), was observed in the heart (Figure 4B).

To confirm this phenomenon, the localization of dscFvs in the tissues was analyzed by immunofluorescence studies (Figure 4E-S). Biotin-labeled dscFvs ($dscFvs^{Bio}$) were intravenously administered to B16BL6 tumor–bearing mice and the tumors, kidneys, and hearts were extracted 2 hours after injection. The $dscFv^{Bio}$ and vascular endothelial cells were stained by streptavidin-AP and anti-CD31 antibody, respectively. In the tumor sections, all of the anti-Robo4 and anti-VEGFR2 $dscFvs^{Bio}$ were clearly detected with CD31+ tumor blood vasculature, whereas anti-His[dscFv]^{Bio} was not detectable (Figure 4E,H,K,N,Q). This finding suggested that both anti-Robo4 and anti-VEGFR2 dscFvs recognized tumor endothelial cells in vivo, which contributed to their accumulation in the tumor. Interestingly, in the kidney and heart sections, signals around CD31+ blood vasculature were detectable only with the anti-VEGFR2 $dscFvs^{Bio}$, and not with anti-Robo4 $dscFvs^{Bio}$ or anti-His[dscFv]^{Bio} (Figure 4F-G,I-J,L-M,O-P,R-S). This finding was compatible with the biodistribution results (Figure 4A-B), which suggested that anti-VEGFR2 dscFvs recognized VEGFR2 on normal blood vessels because VEGFR2 plays an important role in normal tissues, including the kidney and heart.[31-33] No specific accumulation of anti-Robo4 dscFvs was observed in normal tissues, suggesting that the anti-Robo4 mAbs were useful for specific tumor vascular targeting.

Comparison of the cell-internalizing mAbs and low-internalizing mAbs revealed a significantly greater accumulation of cell-internalizing $dscFvs^{125I}$ in the tumors compared with low-internalizing $dscFvs^{125I}$ at 24 hours (Figure 4C-D), whereas no differences were observed at 2 hours (Figure 4A-B). This finding suggested that cell-internalizing mAbs were retained in the tumor for a longer time than the low-internalizing mAbs. This phenomenon was also observed in the kidney and heart with the anti-VEGFR2 dscFvs (Figure 4D). This retention might be caused by the mAb internalization, which allowed the mAb to escape from the bloodstream and accumulate in the tumor blood endothelial cells. Taken together, these results suggest that mAb internalization into the tumor endothelium improves mAb-based drug-delivery in vivo.

Enhanced antitumor effect depends on the cell-internalizing activity

To assess the antitumor potencies of the cell-internalizing mAbs, we selected the scFv-PSIF and IgG-NCS forms. Both forms were suitable models of ADCs because both drugs are used clinically as successful anticancer medicines.[10,43] First, the in vitro cell-killing activities of scFv-PSIFs and IgG-NCSes were estimated by a cytotoxicity assay with MS1 cells (Figure 5A-D). Both forms of cell-internalizing mAbs showed an approximately 10-fold higher cytotoxicity than the low-internalizing mAbs. These findings clearly suggest that internalization enhanced the delivery of conjugated drugs into the cells because our cell-internalizing mAbs and low-internalizing mAbs had similar affinities against antigens (Table 1).

As the therapy experiment in vivo, scFv-PSIFs and IgG-NCSes were intravenously injected into B16BL6 tumor–bearing mice once every 2 days for a total of 5 injections (Figure 5E-H). All cell-internalizing mAbs significantly suppressed tumor growth, whereas the antitumor effects of the low-internalizing antibodies were

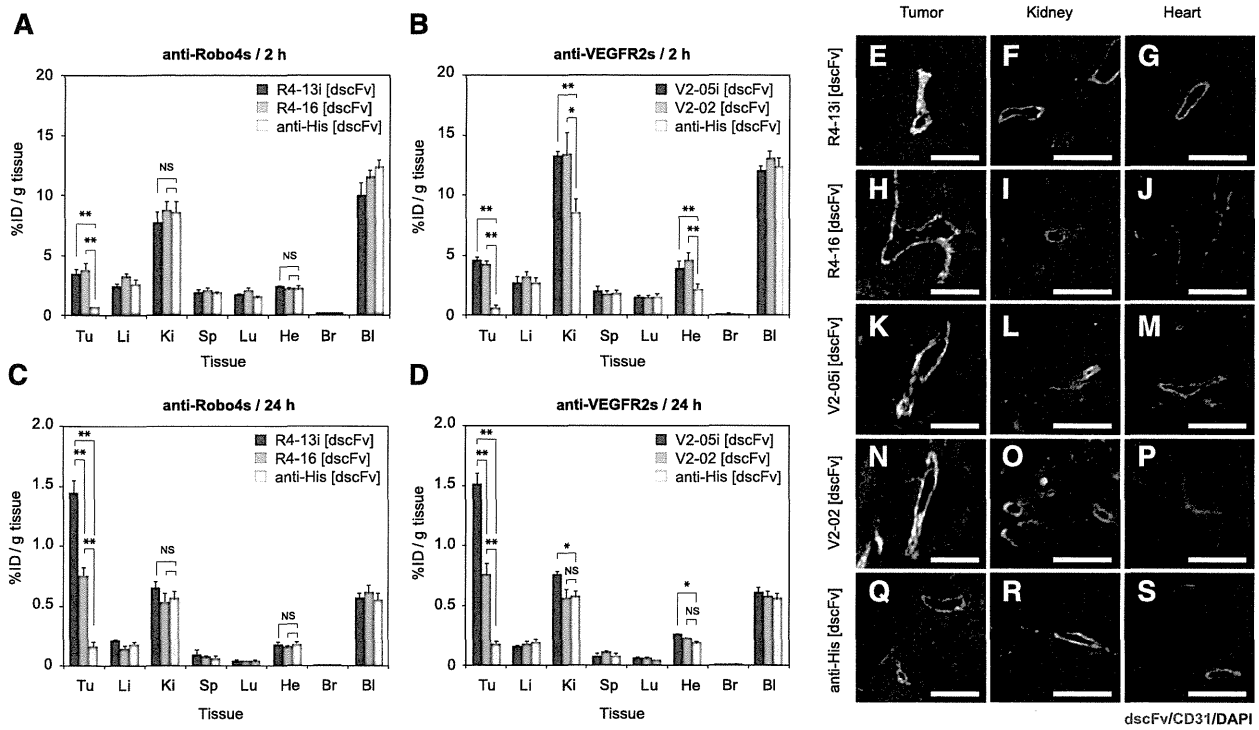

Figure 4. In vivo tumor-targeting activity of cell-internalizing mAbs. (A-D) Biodistribution of dscFvs in B16BL6 tumor–bearing mice. B16BL6 tumor–bearing mice were intravenously administered with anti-Robo4 dscFvs^{125I} (A,C) or anti-VEGFR2 dscFvs^{125I} (B,D). Each organ was extracted after 2 hours (A,B) or 24 hours (C,D), and the radioactivity was measured using a γ counter. %ID/g tissue was calculated using the following formula: %ID/g tissue = (count/g tissue)/(total injected count) × 100 (%). Tu, tumor; Li, liver; Ki, kidney; Sp, spleen; Lu, lung; He, heart; Br, brain; Bl, blood. (A,C) black; R4-13i[dscFv]^{125I}; gray, R4-16[dscFv]^{125I}; white, anti-His[dscFv]^{125I}. (B,D) black, V2-05i[dscFv]^{125I}; gray, V2-02[dscFv]^{125I}; white, anti-His[dscFv]^{125I}. Values are shown as means ± SEM. $*P < .05$; $**P < 0.01$; NS, not significant in Student's *t*-test (n = 11). (E-S) Co-immunostaining of dscFvs with CD31$^+$ blood endothelial cells on the tissue section. B16BL6 tumor–bearing mice were intravenously administered dscFvs^{Bio}. The tumor, kidney, and heart were extracted after 2 hours. Tissue sections of tumor, kidney, and heart were stained with streptavidin-PE conjugate. The blood vasculature was also stained with anti-CD31 antibody. Images were digitally merged. Red, dscFv^{Bio}; green, CD31; blue, DAPI (nucleus); yellow, colocalized region of red and green. Scale bar represents 100 μm. (E-G) R4-13i[dscFv]; (H-J) R4-16[dscFv]; (K-M) V2-05i[dscFv]; (N-P) V2-02[dscFv]; (Q-S) anti-His[dscFv]. (E,H,K,N,Q) Tumor section, (F,I,L,O,R) kidney section, and (G,J,M,P,S) heart section.

similar to those of the negative controls (anti-His[scFv]-PSIF and anti-FLAG[IgG]-NCS). The antitumor effects of R4-13i and V2-05i were similar in both ADC forms. These findings strongly suggest that the cell-internalizing activity of the mAbs was essential to maximize the delivery of the conjugated drug into the target cells, which significantly enhanced the antitumor effect of the ADCs.

Interestingly, the group of mice administered V2-05i[scFv]-PSIF had a significant loss of body weight, whereas the other groups did not (Figure 5I-L). As a preliminary result, 6 of 7 mice died in the V2-05i[scFv]-PSIF group with a similar protocol but with a fourfold higher dosage (60 pmol/mouse), perhaps because of the disruption of VEGFR2-positive cells in normal tissues by V2-05i[scFv]-PSIF, as shown in Figure 4. This side effect was not observed in the V2-05i [IgG]-NCS group. Therefore, we also hypothesized that the toxicity of NCS in normal cells was weak because NCS inhibits DNA synthesis in growing cells, such as tumor cells.[44] At a higher dosage, however, V2-05i[IgG]-NCS carries the risk of side effects. With regard to this point, none of the anti-Robo4 ADCs induced a loss of body weight; therefore, we concluded that Robo4 is a potential target for tumor vascular targeting with ADC.

Discussion

This study led to three novel findings. First, we demonstrated a rapid screening system for cell-internalizing mAbs in combination with the phage antibody library, which accelerated the identification of desired cell-internalizing mAbs. Second, comparative in vivo studies using cell-internalizing mAbs and low-internalizing mAbs with the same affinity values revealed that mAb internalization contributed to tumor targeting and enhanced the antitumor effects of the ADCs. Third, the first in vivo therapeutic application with anti-Robo4 mAb revealed that Robo4 is a therapeutic target on the tumor endothelial cells. The first and second findings will greatly contribute to the development of antibody therapies based on cell-internalizing antibodies such as ADCs, targeted liposomal drugs, or imaging. The third finding provides a new focus regarding the role of Robo4 biology in the body, such as the decreased side effects associated with depleting Robo4-positive endothelial cells in vivo.

This method allowed us to successfully isolate anti-Robo4 and anti-VEGFR2 cell-internalizing mAbs in combination with a phage antibody library and a PSIF-based screening system. This method provided one-step screening of cell-internalization of hundreds of "monoclonal" candidates. This is the main advantage of the present system over the old screening system, which required handling a "polyclonal" pool of mAbs.[6,7] The innovative feature of our method is the use of PSIF as a fusion partner for antibodies in scFv format, thus facilitating the identification of antibody fragments capable of efficient internalization. The scFv fusion is much easier than the chemical conjugation of the antibody to a cytotoxic drug. In principle, this method can be applied to other phage libraries, such as nonimmune phage antibody libraries[35,45] or synthetic